Геология и геофизика, 2021, т. 62, № 5, с. 618—649

ЖАДЕИТИТ И ВЫСОКОЖАДЕИТОВЫЕ ПОРОДЫ В СОСТАВЕ СЕРПЕНТИНИТОВЫХ МЕЛАНЖЕЙ КОМПЛЕКСА РИО-САН-ХУАН (*Доминиканская Республика*): СВИДЕТЕЛЬСТВО ИЗОХИМИЧЕСКОГО ЗАМЕЩЕНИЯ И МЕТАСОМАТИЧЕСКОЙ ДЕСИЛИКАЦИИ МАГМАТИЧЕСКИХ ПРОТОЛИТОВ С ОБРАЗОВАНИЕМ ЖАДЕИТА ПРИ УЧАСТИИ ФЛЮИДА

А. Хертвиг[1], В. Мареш[1], Х.-П. Шертль[1,2]

[1]*Institute of Geology, Mineralogy and Geophysics, Faculty of Geosciences, Ruhr-University Bochum, D-44780 Bochum, Germany*

[2]*College of Earth Science and Engineering, Shandong University of Science and Technology, Qingdao 266590, China*

В статье представлен обзор петрографической, минералогической и геохимической систематики жадеитита и высокожадеитовых пород, образующих блоки в составе серпентинитовых меланжей комплекса Рио-Сан-Хуан (РСХ), Северная Доминиканская Республика. Комплекс РСХ представляет собой остаточное образование субдукционно-аккреционного комплекса Большой Карибской дуги. В прошлом эта дуга занимала пространство между Северной и Южной Америкой, затем переместилась к востоку и заняла свое настоящее положение как дуга Малых Антильских островов; коллизионные фрагменты Большой Карибской дуги сохраняются вдоль двух континентальных окраин. Наша систематическая коллекция включает образцы неоднородного состава от собственно жадеитита (≥90 об.% жадеита) до высококварцевых пород, содержащих жадеит и лавсонит. Среди образцов можно выделить две группы пород. В породах без кварцевой основной массы основным жильным выполнением и промежуточной фазой является альбит, а кварц присутствует только в качестве включений в центральных частях некоторых кристаллов жадеита. В породах с кварцевой основной массой кварц присутствует в больших количествах, в то время как альбит встречается относительно редко. Главный вопрос, связанный с высокожадеитовыми породами: имело ли место осаждение жадеита из водосодержащего флюида высокого давления («жильное осаждение», или тип P), или же формирование высокожадеитовой породы произошло за счет обширного метасоматического замещения магматического протолита (тип R)? В некоторых примерах представлены породы из секущих жил, что явно указывает на принадлежность к типу P. Тем не менее, для большинства образцов классификация неоднозначна. Представленные в данной работе систематизированные результаты петрографического изучения и химического анализа валовых проб жадеитовых пород комплекса РСХ позволяют сделать значительные уточнения. Основной аргумент против формирования жадеитита и высокожадеитовых пород по типу R — это чрезмерная сложность метасоматического массопереноса, необходимого для их образования из любого нормального магматического протолита. Химический анализ валовых проб и состава петрогенных элементов показал, что многие породы с кварцевой основной массой из комплекса РСХ, возможно, образовались в результате изохимического высокобарического низкотемпературного метаморфизма нормальных океанических плагиогранитов, субдуцированных вместе с океанической корой. Кроме того, согласно результатам изоконного анализа, более высокожадеитовые породы, а также породы без кварцевой основной массы также могли сформироваться из подобных плагиогранитов, преимущественно путем непосредственной десиликации, что является весьма вероятным в среде, богатой серпентином. Кварцевые включения в кристаллах жадеита пород без кварцевой основной массы подтверждают гипотезу, согласно которой плагиоклаз плагиогранитного протолита взаимодействует с жадеитом и кварцем. Последующая десиликация и образование альбита в недосыщенной кремнием основной массе породы приводят к появлению характерных реликтовых кварцевых включений в кристаллах жадеита.

Жадеитит, метасоматическое замещение, серпентинитовые меланжы, комплекс Рио-Сан-Хуан, изоконный анализ

JADEITITE AND RELATED ROCKS IN SERPENTINITE MÉLANGES FROM THE RIO SAN JUAN COMPLEX, DOMINICAN REPUBLIC: EVIDENCE FOR BOTH ISOCHEMICAL REPLACEMENT AND METASOMATIC DESILICATION OF IGNEOUS PROTOLITHS WITH FLUID-ASSISTED JADEITE GROWTH

A. Hertwig, W.V. Maresch, H.-P. Schertl

This study presents an overview of the systematic petrography, mineralogy, and geochemistry of jadeitite and jadeite-rich rocks found as blocks in the serpentinite mélanges of the Rio San Juan Complex (RSJC) of the northern Dominican Republic. The RSJC is one of the remnants of the subduction/accretionary complex of the Great Caribbean Arc that once spanned the gap between North and South America, moved relatively eastward to its present position as the Lesser Antilles island arc, and left collisional fragments along the two continental margins. Our systematic collection of heterogeneous samples ranges from *jadeitite s.str.* (sensu stricto) with ≥90 vol.% jadeite to quartz-rich rocks with jadeite and lawsonite. Two suites of rock types can be recognized.

✉e-mail: andreas.hertwig@geow.uni-heidelberg.de

DOI: 10.15372/GiG2021101

In the *matrix-quartz-free* rock suite, albite is the principal vein-filling or interstitial phase. Quartz is present only as inclusions in the cores of some jadeite crystals. In the *matrix-quartz-bearing* rock suite, quartz is abundant and albite is relatively rare. The first-order question concerning jadeite-rich rocks is whether jadeite precipitated from a high-pressure aqueous fluid ("vein precipitation" or "P-type") or whether the jadeite-rich rock formed through comprehensive metasomatic replacement of an igneous protolith ("R-type"). Some examples occur as discordant veins and are clearly P-type. For most, however, classification has been equivocal. The systematic data on the petrography and whole-rock chemistry of jadeite rocks from the RSJC presented in this paper leads to significant clarification. A major argument against R-type genesis is that the metasomatic mass transfer required to produce jadeitite and jadeite-rich rocks from any normal igneous protolith is prohibitively complex. Using whole-rock and major-element compositions, we show that many members of the matrix-quartz-bearing rock suite from the RSJC can be derived by isochemical HP/LT metamorphism of normal oceanic plagiogranites subducted together with oceanic crust. Isocon analysis shows, furthermore, that more jadeite-rich rock types and also members of the matrix-quartz-free suite can be derived from such plagiogranites primarily by straightforward desilication, a realistic scenario in a serpentine-rich environment. The quartz inclusions found in jadeite crystals of the matrix-quartz-free suite corroborate a genetic path in which the plagioclase in a plagiogranite protolith reacts to jadeite + quartz. Later desilication and the formation of albite in the Si-undersaturated rock matrix leave tell-tale quartz inclusions as relics in jadeite crystals.

Jadeitite; metasomatic replacement; serpentinite mélange; Rio San Juan Complex; isocon analysis

INTRODUCTION

Monomineralic aggregates of the mineral jadeite, $NaAl[Si_2O_6]$, are the rarest variety of jade, which has been a material of special significance for artisans worldwide since prehistoric time (Keverne, 2010; Harlow et al., 2014). The material is very tough, hard, and brilliant when polished, which makes it a very desirable raw material for manufacturing tools and for creating highly valued objects of adornment and worship (Keverne, 2010). From the point of view of a petrologist, monomineralic aggregates of the mineral jadeite are called "jadeitite," which represents a rare metamorphic rock type genetically associated with other high-pressure metamorphic rocks, usually in serpentinite-matrix mélange units. About 20 jadeitite occurrences are presently known worldwide (Tsujimori and Harlow, 2012; Harlow et al., 2014). These serpentinite mélanges generally represent exhumed fragments of fossil subduction channels from subduction zones with low geothermal gradients <12 °C/km (see summary by Harlow et al. (2014)). Present ideas on the formation of jadeitite and similar jadeite-rich rocks suggest that these occurrences can provide valuable information on the nature and activity of aqueous fluids in subduction zones. Early petrological studies (see summary by Harlow et al. (2014)), such as in the Polar Urals of Russia (Dobretsov and Ponomareva, 1965) or the Clear Creek, New Idria District in California (Coleman, 1961), concluded that jadeitite formed by comprehensive metasomatic replacement of blocks of original leucocratic igneous or sedimentary rocks in the serpentinite via high-pressure aqueous fluids. This type of genesis has been called "metasomatic replacement" by Yui et al. (2010) or "R-type" (from "replacement") by Tsujimori and Harlow (2012). Coleman (1961) also suggested that jadeitite formed by direct precipitation in veins, and, beginning with their detailed studies on important occurrences in Guatemala, Harlow and coworkers (see summary in Harlow et al. (2014)) stressed and advocated the concept that massive jadeitite generally forms by direct precipitation of jadeite from a high-pressure aqueous fluid. Yui et al. (2010) used the term "vein precipitation," whereas Tsujimori and Harlow (2012) suggest calling these "P-type" (from "precipitation"). Regardless of the assumed mode of formation of jadeitite, it is clear that aqueous fluids must play an important role in their genesis.

Interest in jadeitite has increased considerably in the last 20 years. Harlow et al. (2007) documented about 14 known occurrences worldwide, and five years later Tsujimori and Harlow (2012) extended this list to at least 19 localities. Considerable interest was generated in the Caribbean area by provenance studies on the many lithic and jadeitite artefacts found at sites scattered over a number of widely dispersed islands (Harlow et al., 2006, 2019; García-Casco et al., 2013; Schertl et al., 2018), because such studies allow tracing trading routes of pre-Columbian indigenous peoples (Hofman et al., 2007, 2010, 2011, 2014; Knippenberg, 2007, 2011). Until the discovery of jadeitite occurrences in the Dominican Republic (Schertl et al., 2007, 2012), eastern Cuba (García-Casco et al., 2009; Cárdenas-Párraga et al., 2012), and perhaps central Cuba (Millán and Somin, 1981; Maresch et al., 2012), the classical occurrences in Guatemala already known to Mesoamerican cultures (see summary in Harlow et al. (2014)) were the only known potential sources for Caribbean jade artefacts. In a recent paper, Harlow et al. (2019) studied artefacts from the Bahamas and concluded that several of these must point to an as-yet unknown source. The search continues.

The present paper concentrates on the systematic petrography, mineralogy, and geochemistry of jadeitite and jadeite-rich rocks in the Rio San Juan Complex (RSJC) of the northern Dominican Republic. A major prob-

lem in the provenance studies indicated above is that the potential source areas are extremely heterogeneous in themselves. Unless this heterogeneity is well documented, any comparisons of artefacts with potential source areas will remain indecisive. In addition, previous studies on samples from the RSJC have already shown that this occurrence offers the possibility of contributing to a number of outstanding questions on the nature and genesis of jadeitites worldwide. The RSJC occurrence offers the possibility of studying isolated blocks of jadeitite not only as a regolith on weathered serpentinite outcrops but also as both concordant and discordant veins and layers in blueschist blocks that are themselves entrained in the serpentinite mélanges (Schertl et al., 2007, 2012). Evidence for both P- and R-type genesis can be documented (Hertwig, 2014; Hertwig et al., 2016). A P-type origin is evident in discordant veins crosscutting blueschist blocks in the serpentinite mélange from crack-seal features and arrays of jadeite crystals growing outward from hairline fractures. Hertwig (2014) and Hertwig et al. (2016) studied zircon separated from concordant interlayered jadeitite and blueschist in a block of the mélange as well as from loose blocks of albite–jadeite rock and jadeitite utilizing SIMS U–Pb dating, REE and trace-element analysis, and oxygen isotope study. No zircons were found in the discordant veins. All the rocks studied, both from jadeite-rich samples and the blueschist host of the jadeitite layer, contain magmatic zircon grains that were found to be essentially indistinguishable in age and that can be considered typical of igneous oceanic crust; Hertwig (2014) and Hertwig et al. (2016) suggest inheritance from an igneous protolith and an R-type origin of the jadeite-rich rocks. Actual jadeitite formation might have occurred as much as 40 Myr later, as suggested by younger overgrowths (ca. 78 Ma) on magmatic zircon cores (ca. 117 Ma) separated from the concordant jadeitite layer. Kawamoto et al. (2018) studied fluid inclusions in jadeite, quartz, apatite, and lawsonite from six jadeite-rich rocks in the RSJC, including samples from interlayered jadeitite/blueschist blocks and discordant veins. All the results are similar, regardless of assumed P- or R-type genesis, and point to a pervasive aqueous fluid slightly more saline than seawater (~3.5 wt.% NaCl equiv. (Millero et al., 2008)).

The debate on whether zircon in jadeitite coprecipitated with jadeite from an aqueous fluid at elevated pressures, or represents–at least in part–a relic from an igneous protolith, still continues (Yui and Fukuyama, 2015). Inclusions of jadeite or other high-pressure minerals in zircon can be misleading ("pseudoinclusions"), as discussed by Yui and Fukuyama (2015) and Schertl et al. (2019). Nevertheless, detailed characterization by U–Pb dating, REE and trace-element analysis, and oxygen isotope study corroborates the conclusion that in many jadeitite occurrences the zircon crystals are inherited from an igneous precursor. It has been proposed that zircon crystals were introduced by the high-pressure aqueous fluid as xenocrystals from some igneous precursor in the same mélange (Yui and Fukuyama, 2015; Meng et al., 2016). Whether this suggestion is feasible may be debatable; in the case of the RSJC, the clearly discordant jadeite-rich veins are built up from multiple generations of hairline fractures (Fig. 3*c* in Schertl et al. (2012)). No zircon crystals have so far been detected in such veins, nor does it seem reasonable to expect far-reaching transport in such a crack-seal system. A primary argument that has been offered against a direct comprehensive metasomatic replacement of an igneous precursor (Harlow, 1994; Harlow and Sorensen, 2005; Harlow et al., 2007, 2014) is that such a process should be considered unrealistically complex in terms of the necessary chemical exchange involved. It is the purpose of the present paper to explore this assumption on the basis of the broad spectrum of jadeite-rich rocks we have analyzed in the RSJC. This geochemical and petrographical data base can also be used to address a second remarkable observation. As documented by Harlow et al. (2007, 2014), the most common varieties of jadeitites are silica-undersaturated and albite-bearing. If this is a primary feature, then jadeitite need not necessarily be a high-pressure product. On the other hand, desilication may be secondary and caused by the silica-undersaturated environment provided by encasing serpentinite (Compagnoni et al., 2012).

In a recent paper, Angiboust et al. (2020) present a new, in-depth study of jadeitite occurrences in the Polar Urals, in which they document high-temperature (between 500 and 700 °C) jadeititization of a trondhjemite dike that intruded forearc mantle. The trondhjemite melt was generated by adakite-type partial melting of downgoing oceanic crust. Jadeititization proceeded in the ensuing subsolidus history of the dike via Na–Al fluids initially derived from the subducting slab and later, in the stability field of antigorite, from circulating serpentinizing fluids. Phlogopite-rich schist is a commonly observed product of fluid fluxing at the contact between dike and ultramafic rock. We emphasize here that this scenario differs distinctly from the processes of jadeititization that have so far been described for the RSJC jadeite-rich rocks (Schertl et al., 2012; Hertwig, 2014; Hertwig et al., 2016). U–Pb age dating of zircon in blocks of metamorphosed oceanic crust and jadeitite protoliths, in part as interlayered composites, yields the same ages. The jadeitite protoliths were already a part of the oceanic crust before subduction. Phlogopite, the typical high-temperature blackwall product observed in the Polar Ural example, was observed only in one sample (cf. Table 3) of about 100 discrete jadeite-rich blocks from the RSJC studied in detail. Blackwall alteration assemblages typical of contacts between serpentinite and entrained more siliceous blocks common in many mélanges are also found scattered in the RSJC. However, these assemblages are rich in actinolite and chlorite, indicating formation temperatures lower than 500 °C (Evans, 1977).

GEOLOGIC SETTING

During the Late Jurassic and Early Cretaceous, the North and South American continental plates rifted apart, leading to the formation of oceanic crust in the so-called Proto-Caribbean area and the Gulf of Mexico (Pindell and Kennan, 2009; Pindell et al., 2012; Boschman et al., 2014). Much debate has arisen on the nature of the evolving intraoceanic plate boundary connecting the east-dipping subduction zones of the North and South American Cordillera at the mouth of this widening seaway. Further debate involves the question how an east-dipping subduction zone can realistically evolve into the west-dipping juvenile oceanic island-arc system that will become the intraoceanic Great Caribbean Arc (GCA) system (Pindell et al., 2012) migrating eastward through the space between the two American plates and subducting the Proto-Caribbean oceanic crust (Pindell and Kennan, 2009; Pindell et al., 2012; Boschman et al., 2014). Here we follow the seminal suggestion of Pindell et al. (2012) that the intraoceanic plate boundary might have been a trench–transform–trench system. The GCA then evolved from the bridging transform segment without the necessity of a debatable "flip." Multiple collisions of the eastward-migrating Caribbean Arc with the surrounding continental crustal domains occurred, and remnants of the subduction/accretionary complex of the GCA are now spread out along the entire northern boundary of the Caribbean microplate, in part dismembered by strike-slip faults (Iturralde-Vinent, 1994; Pindell et al., 2005; García-Casco et al., 2009; Flores et al., 2014; Stanek et al., 2019).

The Rio San Juan complex (RSJC) is one of the remnants of the subduction/accretionary complex of the GCA now exposed in the northern Dominican Republic. The RSJC serpentinite mélanges (Fig. 1) formed in the subduction channel of the GCA system and host tectonic blocks of various high-pressure metamorphic rocks, such as different types of blueschist, eclogite, orthogneiss, and subordinate metapelite, marble, and cymrite-bearing and various types of jadeite-rich rocks (Krebs, 2008; Krebs et al., 2011; Schertl et al., 2012). Krebs (2008) and Krebs et al. (2011) provided detailed petrographic descriptions, as well as data on bulk-rock and mineral chemistry, and derived *P–T–t* paths for typical metamorphic blocks from the mélanges. This array of *P–T–t* paths allowed Krebs et al. (Krebs, 2008; Krebs et al., 2011) to describe the dynamics of mass movement in such a subduction channel. The results correlate well with the predictions of the self-organizing 2D numerical subduction-zone model of Gerya et al. (2002), which takes into account the process of continuous hydration

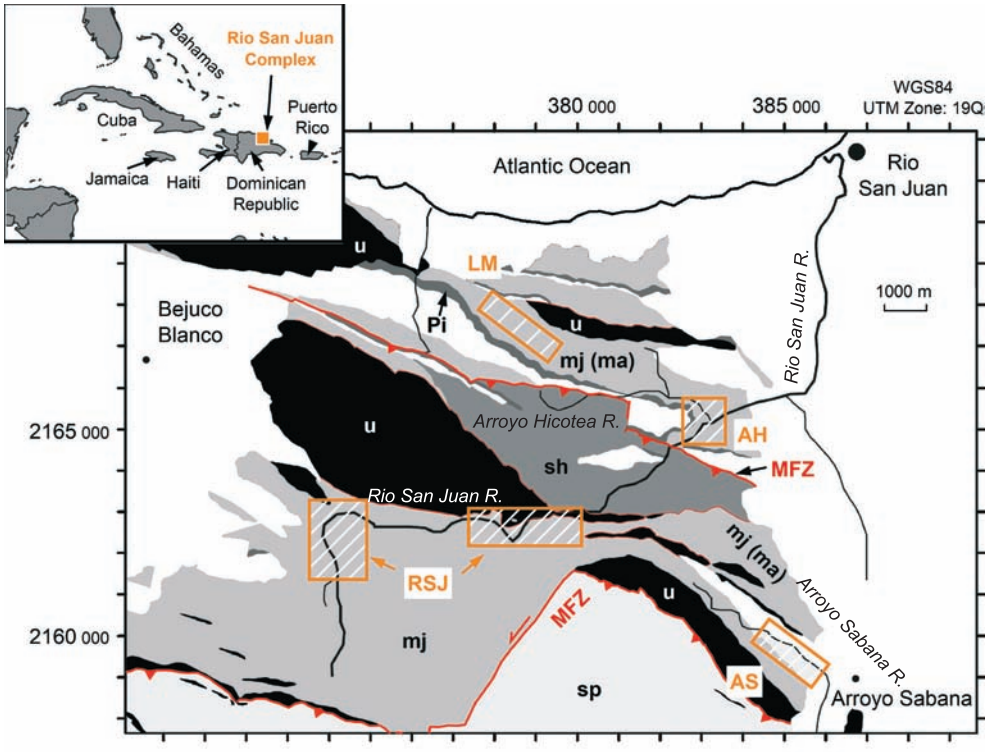

Fig. 1. Geological map of the Rio San Juan Complex showing the Loma Magante (LM), Arroyo Hicotea (AH), Rio San Juan (RSJ), and Arroyo Sabana (AS) sampling locations (u, Gaspar Hernández serpentinites; sh, Hicotea schists; sp, Puerca Gorda schists; Pi, Imbert Formation; mj, Jagua Clara mélange; ma, Arroyo Sabana mélange; MFZ, Morrito Fault Zone); Cenozoic cover is not differentiated; map according to Escuder-Viruete (2010); position of the MFZ as proposed by Escuder-Viruete et al. (2013).

of the mantle wedge and the formation of a dynamically widening serpentinite subduction channel by the fluid released from a kinematically specified subducting plate. Both the petrologically based model and the numerical simulation yield mutual support and provide a coherent picture of a thermally evolving subduction zone. Initiation of subduction is assumed to be at ca. 135 Ma (Pindell et al., 2012), and the subduction zone was active until at least 60 Ma (Krebs, 2008; Krebs et al., 2011). Both clockwise and anticlockwise *P–T* paths for blocks of eclogite can be documented (Krebs, 2008; Krebs et al., 2011), reaching maximum pressure conditions close to the quartz–coesite boundary (ca. 2.5 GPa at 800 °C) during early subduction history. Cooling of the "warm" nascent subduction zone to a mature feature with a dynamic thermal equilibrium at a low *P/T* gradient of 6–7 °C/km was reached at ca. 70 Ma. Garnet- and omphacite-bearing blueschist blocks show only clockwise *P–T–t* paths and maximum *P–T* conditions of 1.2–1.8 GPa and 500–550 °C at around 80 Ma. Jadeite- and lawsonite-bearing blueschist blocks with hairpin clockwise *P–T–t* paths indicate peak metamorphic conditions of 1.5–1.8 GPa at 360–380 °C after 70 Ma. The *P–T* estimates for jadeitite and jadeite-rich rocks from the RSJC vary from 350 to 500 °C and from 1.2 to 1.7 GPa (Schertl et al., 2012; Hertwig, 2014; Hertwig et al., 2016). Such *P–T* conditions were thus first reached between 80 and 70 Ma. This age correlates well with the zircon study of Hertwig (2014) and Hertwig et al. (2016) on jadeite-rich rocks.

SAMPLES

Jadeitites and related jadeite-rich rocks were collected from four main localities situated in the northern (Loma Magante, LM), central (Arroyo Hicotea, AH; Rio San Juan, RSJ), and southeastern sections (Arroyo Sabana, AS) of the Jagua Clara serpentinite mélange (Fig. 1). Since blocks of dense, high-pressure rocks, such as jadeitite, are less susceptible to weathering than the strongly-sheared serpentinite matrix, they are generally not in direct contact with the serpentinite and occur as lag deposits at the surface of weathered serpentinite (LM locality) or as cobbles and boulders in riverbeds (AH, RSJ, and AS localities). The upper reaches of the Rio San Juan River are here of particular importance, because they contain large quantities of boulders that accumulated over time and originated almost exclusively from the surrounding serpentinite mélange. Except for the LM locality, the Jagua Clara serpentinite mélange is not readily accessible, and only sampling along riverbeds (RSJ and AS localities) and flood plains (AH locality) allowed studying a representative area of the central and southern parts of the mélange. Boulders of jadeite-rich rocks in riverbeds are typically smaller than 1 m in diameter; in contrast, blocks resting on hilly terrain can reach several meters. A representative selection of the investigated rock samples discussed in the present study is provided in Table 1. The overwhelming majority of the samples originate from the LM and RSJ localities (Tables 1, 2). Unless noted otherwise, the listed specimens are unique in the sense that they were each taken from individual blocks and boulders to avoid sampling bias.

ANALYTICAL METHODS

Back-scattered electron (BSE) images were acquired using the LEO (Zeiss) 1530 Gemini scanning microscope and the Cameca SX-50 electron microprobe located at Ruhr-University Bochum. Routine mineral analyses using the Cameca SX-50 were performed at 15 kV, 10–15 nA, and a defocused electron beam (5 to 10 µm) to avoid loss of alkali elements. Counting times on background and peak were each 20 s. Data were corrected using the PAP procedure implemented in the Cameca SX-50 software package. The X-ray response was calibrated using the following reference materials: Si, andradite glass; Ti, rutile; Al, spessartine; Fe, andradite glass; Mn, spessartine; Mg, pyrope; Ca, andradite glass; Na, jadeite; and K, K-rich glass. For a subset of samples, the concentrations of some additional elements were acquired: Cr, Cr_2O_3; F, topaz (30 and 60 s counting times on background and peak, respectively); and La and Ce, REE glass (S52SEE3).

Data storage and formula calculation utilized the MINCALC program developed by H.-J. Bernhardt (2010). Formula recalculation of clinopyroxene and assignment of cations to tetrahedral and octahedral sites followed suggestions in Morimoto et al. (1988). After normalizing analyses to four cations, the ratio of Fe^{2+}/Fe^{3+} was estimated by balancing the number of oxygen atoms per formula unit to 6. Mica formulae were based on 11 oxygen atoms per formula unit, and all Fe was treated as Fe^{2+}; the mica nomenclature used in this study is that of Rieder et al. (1998). Amphibole analyses were recalculated on the basis of 23 oxygen atoms per formula unit. For amphiboles, estimation of the amount of Fe^{3+} was done by normalizing the number of cations (excluding Ca, Na, and K) to 13 and applying the procedure described in Leake et al. (1997). The amphibole nomenclature follows recommendations in Hawthorne et al. (2012). The mineral formulae of chlorite and epidote-supergroup minerals were based on 28 and 12.5 oxygen atoms, respectively. In the case of chlorite, all Fe was treated as Fe^{2+}; in the case of epidote-supergroup minerals, all Fe was assumed to be Fe^{3+}.

The whole-rock, major-element data presented in this study (method "m1" in Table 5) were acquired using instruments in the chemical laboratories of Ruhr-University Bochum. Silicon, Ti, Al, Fe_{Tot}, Ca, Mg, Mn, K, Na, and P were determined in glass beads (0.7 g of powdered sample fused with 7 g MERCK Spectromelt®

A 12) by X-Ray fluorescence (XRF) spectroscopy using a PHILIPS PW 2404 instrument. The potentiometric method described by Ungethüm (1965) was used to determine Fe^{3+}/Fe^{2+}. The H_2O content was analyzed by Karl-Fischer titration after dehydration of the samples. The CO_2 content was determined using an ELTRA-CS-500 carbon sulfur analyzer.

Trace-element data represent a compilation of data acquired at Ruhr-University Bochum and Acme Analytical Laboratories (methods "t1" or "t2," respectively in Table 5). Lithium was analyzed in selected samples by atomic-absorption spectroscopy (AAS) using a VARIAN AA 300 at Ruhr-University Bochum (sample digestion: 1 mL HF (48%) and 5 mL HNO_3 (65%); water bath at 80 °C for several hours). Barium, Cd, Cl, Cr, Cu, F, Mo, Nb, Ni, Pb, Rb, S, Sb, Sr, Zn, Zr, and Y were analyzed in pressed powder discs (8 g sample material + 2 g Elvacit®) by XRF using a PHILIPS PW 2404 hosted at Ruhr-University Bochum (USGS Rock Stan-

Table 1. **Selection of jadeite rocks discussed in this study**

Samples	Locality*	Rock suite**	Abbrev. rock name***	Rock name	Notes
25255	AH	b	JLQ	Jadeite–lawsonite quartzite	
26320/21	LM3	b	dJLQ	Jadeite–lawsonite quartzite	Discordant JLQ, samples from one block
26322	LM3	f	Jdt s.str.	Jadeitite s.str.	
30023	LM1	f	Jdt s.str.	Jadeitite s.str.	
30045	LM2	–	JBS	Jadeite blueschist	BS block
30046	LM2	b	Jdt s.str.	Jadeitite s.str.	Part of the BS block (30045)
30065	LM1	f	Jdt	Jadeitite	
30066	LM1	f	Jdt	Phengite-rich jadeitite	
30071	RSJ2	f	Jdt	Jadeitite	
30083	LM2	f	Jdr	Phengite–jadeite rock	
30092	LM3	b	JLQ	Garnet-bearing jadeite–lawsonite quartzite	
30101	LM3	b	dJLQ	Jadeite–lawsonite quartzite	Discordant JLQ
30105	LM3	b	dJLQ	Jadeite–lawsonite quartzite	Discordant JLQ
30106	LM3	b	dJLQ	Jadeite–lawsonite quartzite	Discordant JLQ
30108	LM3	f	Jdt	Jadeitite	
30765	LM2	f	Jdr	Glaucophane-bearing phengite–jadeite rock	
30766	LM2	f	Jdr	Albite–jadeite rock	
30769	LM1	f	Jdr	Albite-rich phengite–jadeite rock	
30772b	LM2	b	JLQ	Jadeite–lawsonite quartzite	Concordant JLQ layers in jadeite blueschist
30787	LM2	b	dJLQ	Garnet-bearing jadeite–lawsonite quartzite veinlet	Discordant JLQ
30790b	LM2	f	Jdr	Albite–jadeite rock	
30799	LM3	b	JLQ	Jadeite–lawsonite quartzite	
30804	LM3	b	JLQ	Jadeite–lawsonite quartzite	
30823/24	LM4	f	Jdt	Paragonite-bearing jadeitite	Samples from one block
30846	RSJ1	f	Jdr	Phengite-rich omphacite–jadeite rock	
30852	RSJ1	f	Jdt s.str.	Jadeitite s.str.	
30853	RSJ1	f	Jdr	Phengite-rich omphacite rock	
30858	RSJ1	b	LQ	Lawsonite quartzite	
30871	AS	f	Jdr	Phengite–jadeite rock	
30999	AH	f	Jdr	Jadeite–albite rock	
31005	AH	f	Jdr	Pumpellyite- and lawsonite-rich jadeite rock	
31034	RSJ6	f	Jdt s.str.	Jadeitite s.str.	In contact with jadeite blueschist
31049	RSJ6	f	Jdt s.str.	Jadeitite s.str.	
31074	RSJ4	f	Jdt	Jadeitite	

* Abbreviated sample locality; for details see Table 2.

** b, matrix-quartz-bearing rock suite; f, matrix-quartz-free rock suite.

*** JBS, Jadeite blueschist; Jdr, jadeite rock; Jdt, jadeitite; Jdt s.str., jadeitite sensu stricto; JLQ, jadeite–lawsonite quartzite; dJLQ, discordant jadeite–lawsonite quartzite; LQ, lawsonite quartzite.

Table 2. **Locations of samples and outcrop conditions**

Locality		Outcrop	UTM Coordinates*	Notes
Loma Magante	LM1	Blocks along or adjacent to the path that branches off from the main street and leads up to the Loma Magante hill	377900 2168100	Mostly blocks on path
	LM2		378300 2167400	East of path, northeast-facing flank of Loma Magante
	LM3		378400 2166900	West of path, southwest-facing flank of Loma Magante
	LM4		379600 2167000	Approx. 800 m northeast from highest elevation (when walking on path)
Rio San Juan	RSJ1	Boulders in the river beds of the Rio San Juan River and its tributaries	374400 2163000	At the river bend of the Rio San Juan River
	RSJ2		374000 2162100	Approx. 900 m south of river bend
	RSJ4		374000 2161200	Tributary at the upper reaches of the Rio San Juan River
	RSJ6		379600 2162900	Lower course of the Rio San Juan River; flat terrain
Arroyo Sabana	AS	Boulders in the river bed of the Arroyo Sabana River	385400 2159400	
Arroyo Hicotea	AH	Blocks in grassy and hilly terrain; flood plain close to the confluence of the Rio San Juan and Arroyo Hicotea Rivers	383200 2165300	

* WGS84, UTM Zone 19Q.

dards: RGM-1 and STM-1). The concentrations of Ba, Be, Co, Cs, Ga, Hf, Nb, Rb, Sn, Sr, Ta, Th, U, V, W, Zr, Y, and La–Lu (lithium metaborate/tetraborate fusion and subsequent dilute nitric digestion) were determined using ICP MS in the laboratories of AcmeLabs. For information on mean detection limits for trace-element analysis see Appendix EA1.

RESULTS

Naming conventions and definition of rock suites

The block inventory of the Jagua Clara serpentinite mélange comprises a huge variety of *jadeite-rich* (vol.% Jd ≥ 10) rocks, with many blocks being heterogeneous on a macroscopic scale. The jadeite-rich rocks of this study are broadly divided into two rock suites, based on the presence of quartz in the rock matrix. In the *matrix-quartz-free* rock suite, albite is the principal vein-filling or interstitial phase. Although quartz is virtually absent in this rock suite, a critical feature is that quartz does occur as small mineral inclusions within jadeite in many of the rocks, as will be discussed later in greater detail. Members of the *matrix-quartz-bearing* rock suite contain abundant quartz, and albite is relatively rare.

Jadeite contents of ≥90 vol.% have been traditionally used to define and distinguish jadeitite from other associated rocks (Harlow, 1994). While there are samples in our collection that are reasonably homogeneous and jadeite-rich enough to be classified as jadeitite according to this definition (e.g., samples 30023 and 30046, see Tables 1, 3), either most samples are too heterogeneous on the macroscopic scale, or the jadeite contents do not reach 90 vol.%, or both. Acknowledging this traditional definition, we define rocks containing ≥90 vol.% jadeite as *jadeitite s.str.* (sensu stricto). Acknowledging also the recommendations of the International Union of Geological Sciences, samples with 75 ≤ vol.% Jd ≤ 90 are also classified as *jadeitite,* but without the sensu stricto suffix. This is particularly applicable in the case of the matrix-quartz-free rock suite. The jadeite-rich rocks of the matrix-quartz-bearing rock suite with jadeite contents <90 vol.% are classified as *jadeite–lawsonite quartzite* (JLQ), *jadeite quartzite* (JQ), or *lawsonite quartzite* (LQ) according to the relative proportions of the major mineral constituents. For simplicity of expression, all types of jadeite-rich rocks will be summarily referred to as *jadeite rocks* in this paper.

PETROGRAPHIC DESCRIPTION

Macroscopic rock fabric and appearance in hand specimen

Boulders in riverbeds are rounded and exhibit mostly smooth surfaces with thin (<3 mm) weathering crusts. Blocks located within serpentinite are more angular to subrounded and, in rare cases, are encrusted with various mineral aggregates. So far, no block has been found in direct, *primary* contact with the sheared serpentinite matrix. Jadeite rocks appear pale to grayish green (Fig. 2*a*, *b*), greenish gray, or dark green (Fig. 2*c*), with the color being a function of the relative modal abundances of jadeite, omphacite, epidote-supergroup minerals,

Table 3. **Modal proportions in jadeite rocks of this study**

Samples	Rock suite*	Abbrev. rock name**	Jd	Omp	Ab	Qtz	Cal	Phg	Pa	Bt	Chl	Gln	Lws	Grt	Ep/ Czo	Ap	Ttn	Zrn	Opaque phases	Notes
25255	b	JLQ	++	m	acc.	++		m			acc.		+							
26320/21	b	dJLQ	++	acc.		+		m			acc.	acc.	+				acc.	acc.		
26322	f	Jdt s.str.	++++	m	m			m									m			Qtz incl. in Jd
30023	f	Jdt s.str.	++++		m		m	acc.			m		acc.		acc.					Lws, Ab incl. in Jd
30046	b	Jdt s.str.	++++		acc.	m	m	m				m				acc.	acc.	acc.		
30065	f	Jdt	+++	m	+			acc.			m				acc.		acc.	acc.		Qtz incl. in Jd
30066	f	Jdt	+++	acc.	m		m	+								acc.	m	acc.		Rt enclosed by Ttn
30071	f	Jdt	+++	m	m			m		m					m	acc.	acc.	acc.		
30083	f	Jdr	++		m		+	+				acc.					acc.			
30092	b	JLQ	++			+		acc.			acc.		+	m			m			
30101	b	dJLQ	+	m		+		m				acc.	++			acc.	acc.			
30105	b	dJLQ	+	acc.	acc.	++		m				acc.	+			acc.	acc.			
30106	b	dJLQ	++ (Jd + Omp)		acc.	+		acc.					+	acc.		acc.	acc.		acc.	Rt enclosed by Ttn
30108	f	Jdt	+++	acc.	m			acc.			m				acc.	acc.	acc.		acc.	Anl
30765	f	Jdr	++	acc.	m			+			acc.	+				acc.	m			Rt enclosed by Ttn
30766	f	Jdr	++		+		+	acc.			m	acc.	acc.		acc.			acc.	m	
30769	f	Jdr	++		+		m	+							acc.	acc.	m			Qtz incl. in Jd and Cal
30772b	b	JLQ	+	acc.	acc.	++		m			acc.	acc.	+				acc.			
30787	b	dJLQ	++			+		acc.				acc.	m	+			m			
30790b	f	Jdr	++	m (Agt)	+		+	acc.			m	acc.			m		m	acc.	m	Qtz incl. in Jd
30799	b	JLQ	+		acc.	++		m			acc.	m	+		acc.		m		acc.	
30804	b	JLQ	++		acc.	+		m				acc.	++		acc.				m	
30823/24	f	Jdt	+++	(i)	acc.			m	m		m		+		m		m	acc.		
30846	f	Jdr	++	+	m			+		acc.	acc.				+	acc.	acc.	acc.		
30852	f	Jdt s.str.	++++	(i)	m					m					acc.		acc.			Phl
30853	f	Jdr	m	++	+		m	++									acc.		acc.	
30858	b	LQ			acc.	+++		m					+	m	m		acc.		acc.	
30871	f	Jdr	++	+	m			+							m		acc.	acc.	m	
30999	f	Jdr	+	acc.	+		+	+			+				m		m			
31005	f	Jdr	++	m	+			acc.			m		+		m	m	acc.			+ Pmp (10 vol.%)
31034	f	Jdt s.str.	++++	acc.	m						m	acc.					m			Qtz incl. in Jd
31049	f	Jdt s.str.	++++	m	acc.			m			acc.	acc.	acc.		acc.		m			
31074	f	Jdt	+++	m	m		acc.			m					acc.		m			Anl

++++, vol.% ≥ 90
+++, 75 ≤ vol.% < 90
++, 40 ≤ vol.% < 75
+, 10 ≤ vol.% < 40
m, 1 ≤ vol.% < 10
acc. = accessory amounts
(i) intergrown with jadeite
* b, matrix-quartz-bearing suite; f, matrix-quartz-free suite.
** See Table 1.

Ab, albite; Agt, aegirine-augite; Anl, analcime; Ap, apatite; Bt, biotite; Cal, calcite; Chl, chlorite; Ep/Czo, epidote-supergroup minerals; Gln, glaucophane; Grt, garnet; Jd, jadeite; Lws, lawsonite; Omp, omphacite; Pa, paragonite; Phg, phengite; Phl, phlogopite; Pmp, pumpellyite; Qtz, quartz; Rt, rutile; Ttn, titanite; Zrn, zircon.

and chlorite. In the case of monomineralic rocks, the overall color is dependent on the composition of the jadeitic clinopyroxene: The higher the molar amount of the jadeite endmember in clinopyroxene, the more whitish the color that is observed in hand specimen.

The samples of the matrix-quartz-free suite are mostly fine- to medium-grained and massive (Fig. 2*a, b*) but also slightly to strongly foliated (Fig. 2*c, d*). Veins filled with albite, calcite, or both are common. Roughly half of the samples of this suite exhibit roundish to irregular-shaped dark green mineral aggregates (Fig. 2*b*) that are mainly composed of epidote-supergroup minerals + chlorite/biotite, chlorite alone, or albite + omphacite assemblages. So far, only one matrix-quartz-free jadeite rock has been found in contact with a glaucophane-rich rock (sample 31034, Fig. 2*d*). Rocks of the matrix-quartz-bearing suite can form concordant layers (*jadeitite s.str.*, sample 30046, Fig. 2*e*; jadeite–lawsonite quartzite, sample 30772 (Fig. 2*f*)) within blueschists or discordant veins (e.g., jadeite–lawsonite quartzite, sample 30101, Fig. 2*g*) that crosscut the foliation of the blueschist blocks; isolated blocks of matrix-quartz-bearing samples also exist. Jadeite rocks can appear slightly translucent when modal amounts of quartz are high (Fig. 2*h*). The minerals are heterogeneously distributed, and lawsonite, omphacite/jadeite, and quartz form schlieren and clusters in the discordant jadeite–lawsonite quartzites (Fig. 2*g*), whereas the minerals are homogeneously distributed in the concordant jadeitite and jadeite–lawsonite quartzite.

The matrix-quartz-free suite: mineralogy and microscopic rock fabric

Most of the jadeite rocks of the matrix-quartz-free suite are best described as roughly granoblastic (Fig. 3*a, b*). If present, the foliation observed in hand specimen and thin section results from partly oriented, platy crystals (Fig. 3*b*), homeoblastic layers of jadeitic clinopyroxenes of different grain sizes, and phyllosilicates (Fig. 3*c*). The frequently observed morphologic features of jadeite include euhedral to subhedral grain shapes (Fig. 3*d*), especially when in contact with albite in interstitial spaces (Fig. 3*e, f*), oscillatory or rhythmic zonation pattern (Fig. 3*f*), xenoblastic, inclusion-rich grains and aggregates (Fig. 3*g, h*), and cloudy, inclusion-rich cores surrounded by transparent, inclusion-poor rims (Fig. 3*d*). Albite, analcime, calcite, epidote-supergroup minerals, lawsonite, phengite, and quartz have been observed as inclusions in jadeite so far. Figures 4*a–f* show BSE images and X-ray elemental maps of two matrix-quartz-free rocks that contain jadeite exhibiting minute quartz inclusions. The inclusions are generally small (<5 μm) and are in some cases accompanied by oriented inclusions made of other minerals, for instance, calcite. In samples similar to 30065, there is evidence for incomplete reaction of jadeite and quartz, resulting in the formation of albite at the interface between jadeite host and inclusion (Fig. 4*b*). The inclusion assemblage in the cloudy cores of jadeite in sample 30023 comprises albite, lawsonite, white mica, and titanite (Fig. 4*g*).

Omphacite is a common, both minor or major mineral constituent in jadeite rocks of this suite. Frequently observed are euhedral to subhedral omphacite overgrowths on jadeite in proximity to albite-filled veins and interstitial fillings (Figs. 3*e*, 5*a*). In some samples, individual omphacite grains form cores embedded in jadeitic clinopyroxene (Fig. 5*b*), or omphacite occurs as very fine-grained and oriented inclusions in jadeite (see section on mineral chemistry). Albite is anhedral and the dominant phase in interstitial fillings, veins, and lenticular mineral aggregates in all rocks of the matrix-quartz-free suite. Phengite is the predominant mica and present in accessory or minor amounts in most of the jadeite rocks. In rare cases, phengite is the second most abundant phase after the jadeitic clinopyroxenes (sample 30853). Paragonite has been observed only in two samples of this suite so far (samples 30823/24). Most biotite (green in thin section under plane-polarized light) forms dark green mineral aggregates together with zoned and euhedral epidote-supergroup minerals (Fig. 5*c*). The latter also occur finely dispersed in rock matrixes (Fig. 3*c*). Chlorite is often observed together with epidote-supergroup minerals, but sometimes chlorite only fills interstitial spaces between jadeite grains (Fig. 5*d*). Calcite is present as an important vein-filling phase together with albite, as inclusions in jadeite, and occasionally as euhedral crystals in contact with albite. Additional phases are (in accessory or minor amounts, in alphabetical order): analcime, apatite, galena, glaucophane, hematite, lawsonite, pumpellyite, pyrite, rutile, titanite, and zircon.

The matrix-quartz-bearing suite: mineralogy and microscopic rock fabric

The jadeite of the matrix-quartz-bearing suite exhibits a range of grain shapes; euhedral to subhedral crystals (Fig. 6*a, c, d*) are observed as well as aggregates of anhedral crystals (Fig. 6*b, g*). Of note are prismatic jadeite crystals that are oriented perpendicular to cracks, indicating fluid-mediated crystal growth (Fig. 6*d*), as well as jadeite-rich nodules surrounded by omphacite (Fig. 6*e*); both morphologies are present only in the discordant jadeite–lawsonite quartzite lithology. Oscillatory or rhythmic zonation patterns in jadeite are less common in this rock suite. Quartz is the principal phase filling interstitial spaces (Fig. 6*a*) and the main constituent of the rock matrix (Fig. 6*c, g*). Polygonal aggregates of quartz exhibit different degrees of undulatory extinction. The matrix-quartz-bearing rocks typically contain 10 to 60 vol.% of lathlike lawsonite; poikiloblasts enclosing minute quartz inclusions are common (Fig. 6*c*). Glaucophane, an important accessory and minor

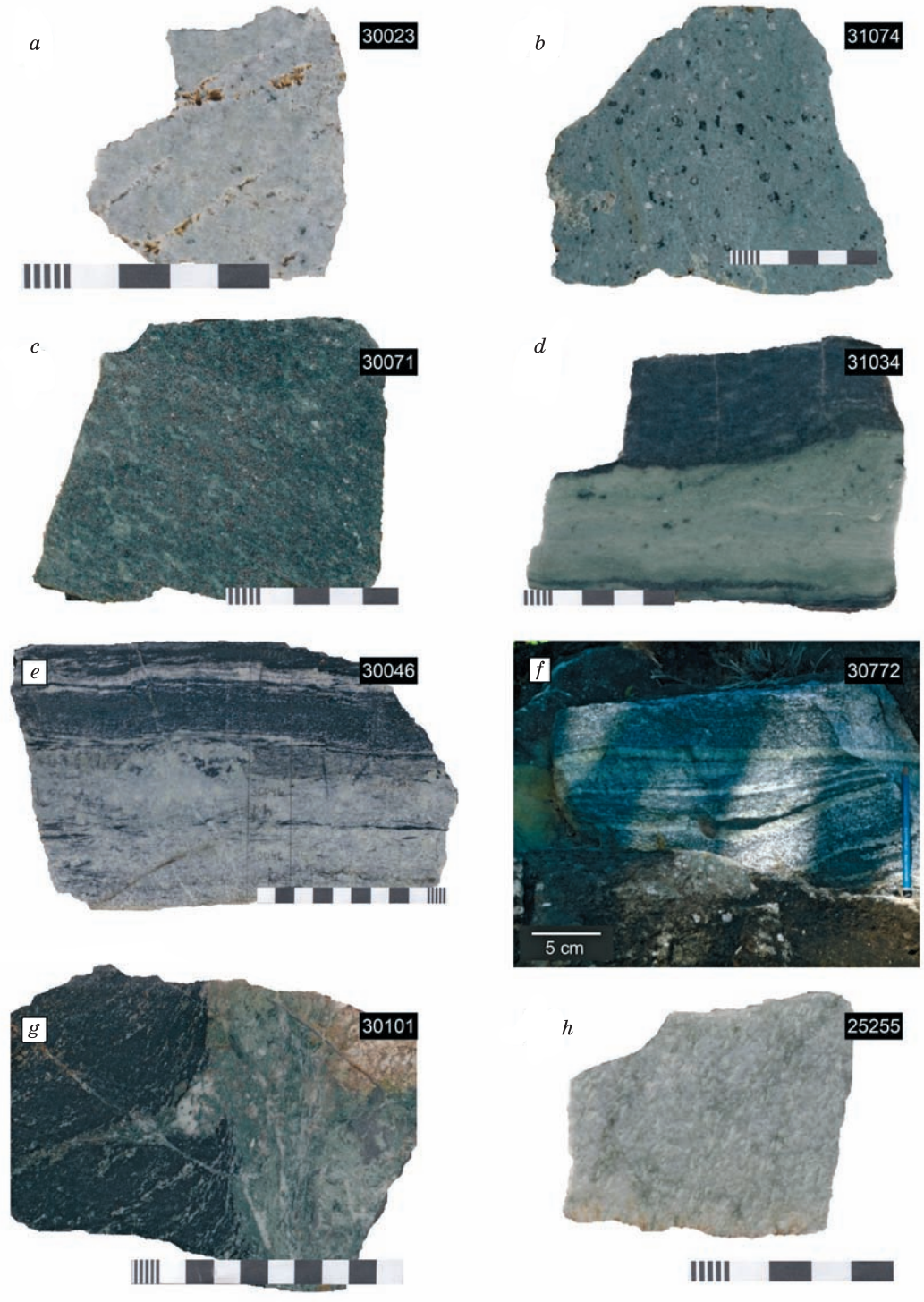

Fig. 2. Representative hand-specimen photographs of matrix-quartz-free (*a–d*) and matrix-quartz-bearing (*e–h*) jadeite rocks (scale bar in *a–d* and *h*, 5 cm; in *e* and *g*, 10 cm).

a, Greenish white to pale green massive jadeitite with open cracks and cavities; *b*, grayish green massive jadeitite, roundish dark green mineral aggregates (chlorite and epidote); *c*, dark green foliated mica-rich jadeitite; *d*, intense green foliated *jadeitite s.str.* adjacent to a chlorite–jadeite blueschist; *e*, quartz-bearing *jadeitite s.str*. in contact with jadeite–blueschist country rock; *f*, outcrop photograph of the concordant jadeite–lawsonite quartzite (bright layers) alternating with glaucophane- and jadeite-rich layers; *g*, discordant jadeite–lawsonite quartzite exhibiting quartz-, lawsonite-, and jadeite/omphacite-rich mineral clusters; *h*, pale green massive jadeite–lawsonite quartzite.

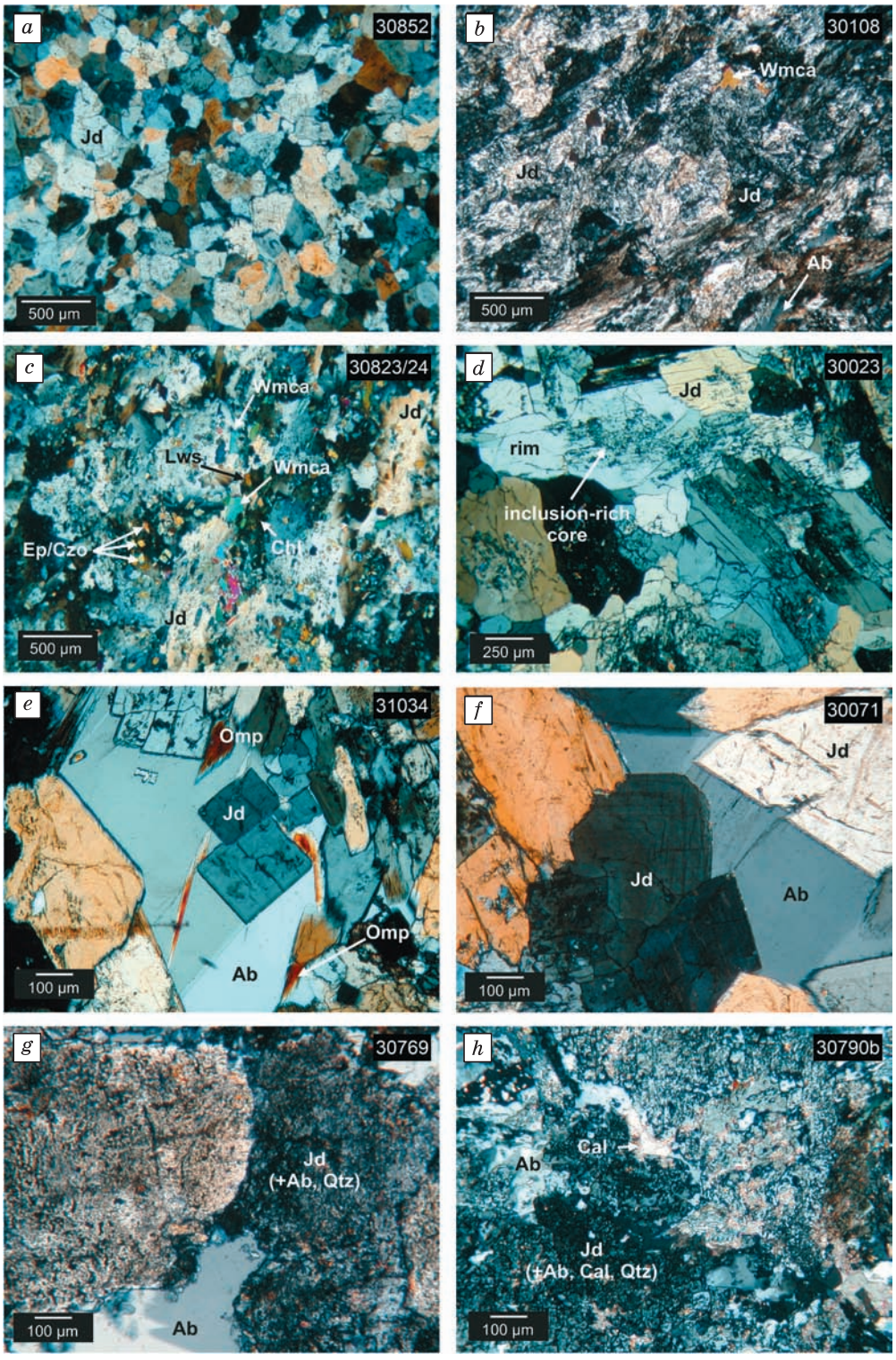

Fig. 3. Photomicrographs of thin-sections of matrix-quartz-free jadeite rocks (crossed polarizers).

a, Inclusion-poor jadeite grains in granoblastic texture; *b*, inclusion-rich anhedral, slightly elongated jadeite crystals; *c*, inclusion-rich anhedral jadeite grains with undulatory extinction; *d*, subhedral jadeite crystals exhibiting inclusion-rich cores (see also Fig. 4*g*) and transparent rims; *e*, euhedral jadeite crystals with omphacite overgrowths enclosed by interstitial albite (see also Fig. 7*a*); *f*, subhedral oscillatory-zoned jadeite grains and interstitial albite; *g*, anhedral jadeite grains with a multitude of inclusions; *h*, anhedral jadeite crystals with variably sized inclusions (see also Fig. 4*f*). Ab, Albite; Cal, calcite; Chl, chlorite; Ep/Czo, epidote-supergroup minerals; Jd, jadeite; Lws, lawsonite; Omp, omphacite; Qtz, quartz; Wmca, white mica.

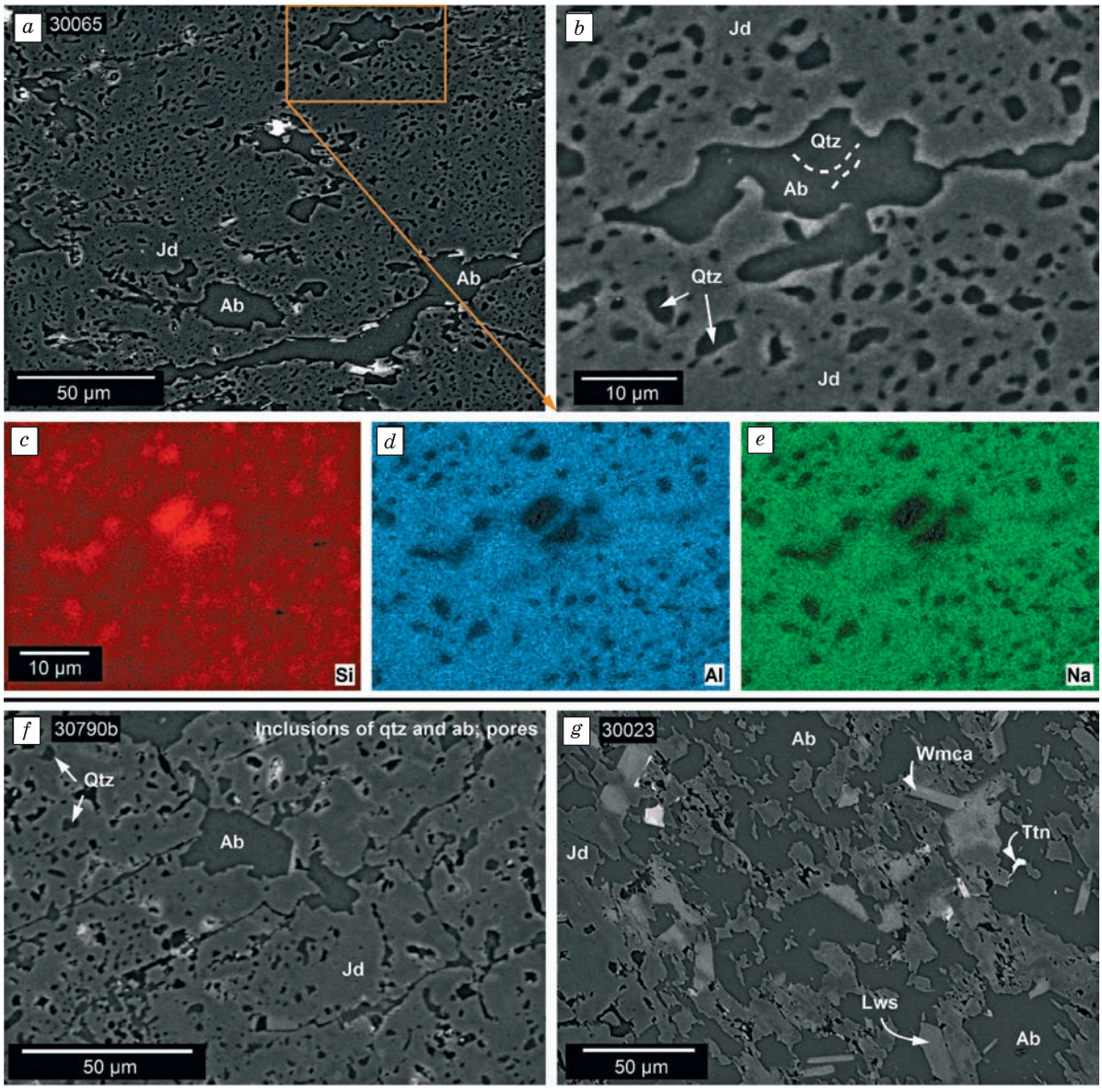

Fig. 4. Back-scattered electron (BSE) images (*a*, *b*, *f*, and *g*) and X-ray element maps (*c*–*e*) of mineral inclusion assemblies in jadeite.

a–*e*, Albite encloses quartz inclusions in jadeite; *f*, albite and quartz inclusions in jadeite; *g*, various mineral inclusions in cloudy, inclusion-rich jadeite core. Ttn, Titanite; other mineral abbreviations as in Fig. 3.

phase, shows euhedral to subhedral morphology, for instance, in the glaucophane-rich layers of concordant jadeite–lawsonite quartzite (sample 30772) and forms fibrous aggregates in the jadeite-rich portions of the same rock (Fig. 6*f*). In the jadeite blueschist (sample 30045) hosting the concordant jadeitite (sample 30046), glaucophane blasts are surrounded by a fine-grained aggregate of jadeitic clinopyroxenes. Albite is present in these rocks as a fine-grained replacement product of jadeite (Fig. 6*g*). Additional phases are (in accessory or minor amounts, in alphabetical order): apatite, calcite, chlorite, garnet (almandine, anhedral and fragmented), opaque phases, phengite, rutile, titanite, and rarely zircon.

Mineral chemistry

Figure 7 shows BSE images of jadeite rocks of both suites. The numbered dots indicate the locations of the respective analyses in Table 4 and in the clinopyroxene triangular diagram shown in Fig. 8. Clinopyroxenes analyzed in both rock suites belong either to the Na- or Ca–Na pyroxene groups (Morimoto et al., 1988) and

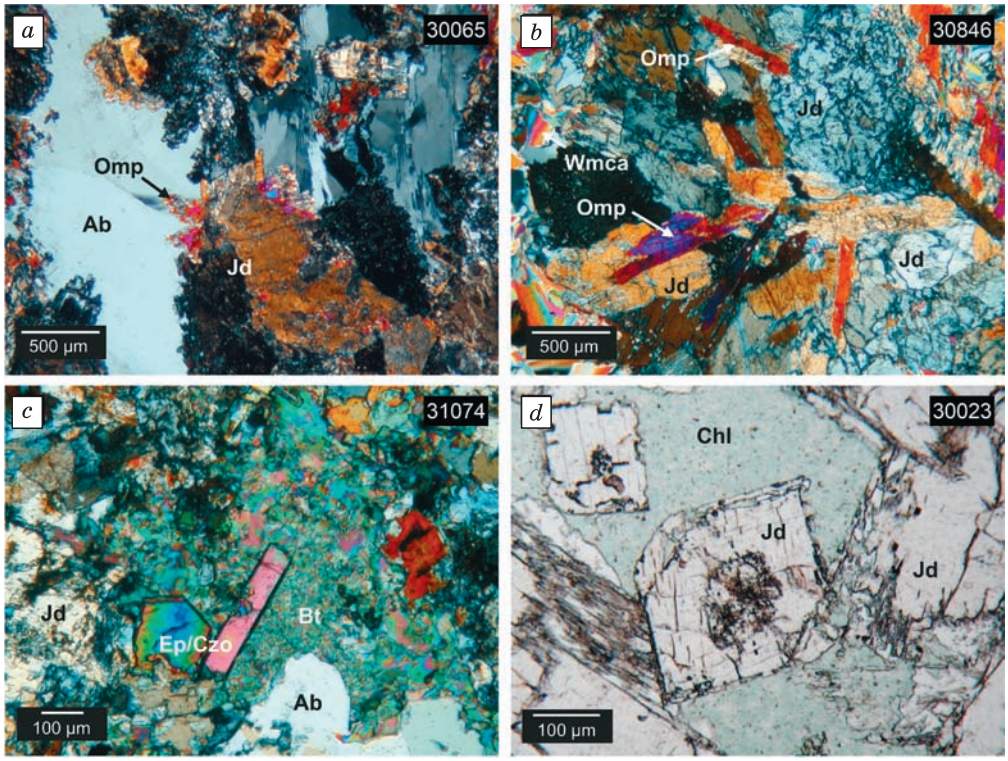

Fig. 5. Microphotographs of thin-sections of matrix-quartz-free jadeite rocks (crossed polarizers: *a–c*; plane-polarized light: *d*).

a, Omphacite overgrowths on jadeite; *b*, omphacite cores enclosed in jadeite grains; *c*, euhedral epidote/clinozoisite crystals embedded in very fine-grained biotite; *d*, euhedral jadeite crystal and interstitial, fine-grained chlorite. Bt, Biotite; other mineral abbreviations as in Fig. 3.

their chemical variations can be expressed in terms of the jadeite (Jd), aegirine (Ae), diopside (Di), and hedenbergite (Hd) endmembers; Al occupying tetrahedral sites is ≤0.01 atoms per formula unit (a.p.f.u.). To a first approximation, jadeitic clinopyroxenes of the matrix-quartz-bearing suite are closer in composition to the jadeite endmember (up to Jd_{100}, typically $Jd_{95}Ae_0Di_4Hd_1$ to $Jd_{87}Ae_5Di_5Hd_3$) and contain less aegirine component ($Ae_{<10}$) compared to those of the matrix-quartz-free suite (typically $Jd_{85\text{-}95}$ and $Ae_{<30}$). The chemical compositions of omphacite overgrowths and cores in jadeite (Fig. 7*a–c*) are typically $Jd_{40\text{-}50}Ae_{0\text{-}10}Di_{40\text{-}45}Hd_{5\text{-}10}$. Of note are oriented intergrowths of fine-grained omphacite and jadeite in samples 30823 and 30852 (Fig. 7*d*, *e*) as well as the exceptional occurrence of aegirine–augite-bearing assemblages in sample 30790b (Fig. 7*f*). In the matrix-quartz-bearing suite, omphacite is observed almost exclusively in the discordant jadeite–lawsonite quartzite lithology, where omphacite rims jadeite-rich nodules (Fig. 7*h*), forms whole nodules, and is sometimes a component of rhythmic zoning patterns in clinopyroxenes.

Most variations in the mineral chemistry of white mica can be expressed in terms of the aluminoceladonite, paragonite, and trioctahedral substitutions (Fig. 9). Deviations from exchange vectors of these substitutions might be due to the incorporation of Fe^{3+}. Most of white mica is phengite (typically $3.2 < Si < 3.7$ a.p.f.u.); sodium contents are low ($Na < 0.2$ a.p.f.u.). Sample 30823 contains two different generations of paragonite (Na ~0.95 and ~0.84 a.p.f.u.). Typical chlorite analyses yielded X_{Mg} values ranging from 0.4 to 0.8. Iron-rich chlorite (X_{Mg} ~0.3, chamosite) was observed in contact with Fe-sulfide in sample 30108. In addition to the homovalent Mg–Fe^{2+} exchange, chlorite chemistry is governed by the Tschermak's exchange (Fig. 10*a*). Variations in the compositions of epidote-supergroup minerals are readily explained by the homovalent Al–Fe^{3+} exchange linking the clinozoisite/zoisite and epidote endmembers (Fig. 10*b*). Exceptions are the analyses made in sample 30769 that show significant contributions of the (La, Ce)-allanite endmember (Fig. 10*b*, inset). Sodium amphibole is glaucophane or ferro-glaucophane ($0.4 < X_{Mg} < 0.8$, Fig. 11).

Whole-rock geochemistry

Figure 12 illustrates the most notable differences between the matrix-quartz-free and -bearing rock suites in terms of major-element geochemistry. The matrix-quartz-free rocks generally possess lower SiO_2 and higher

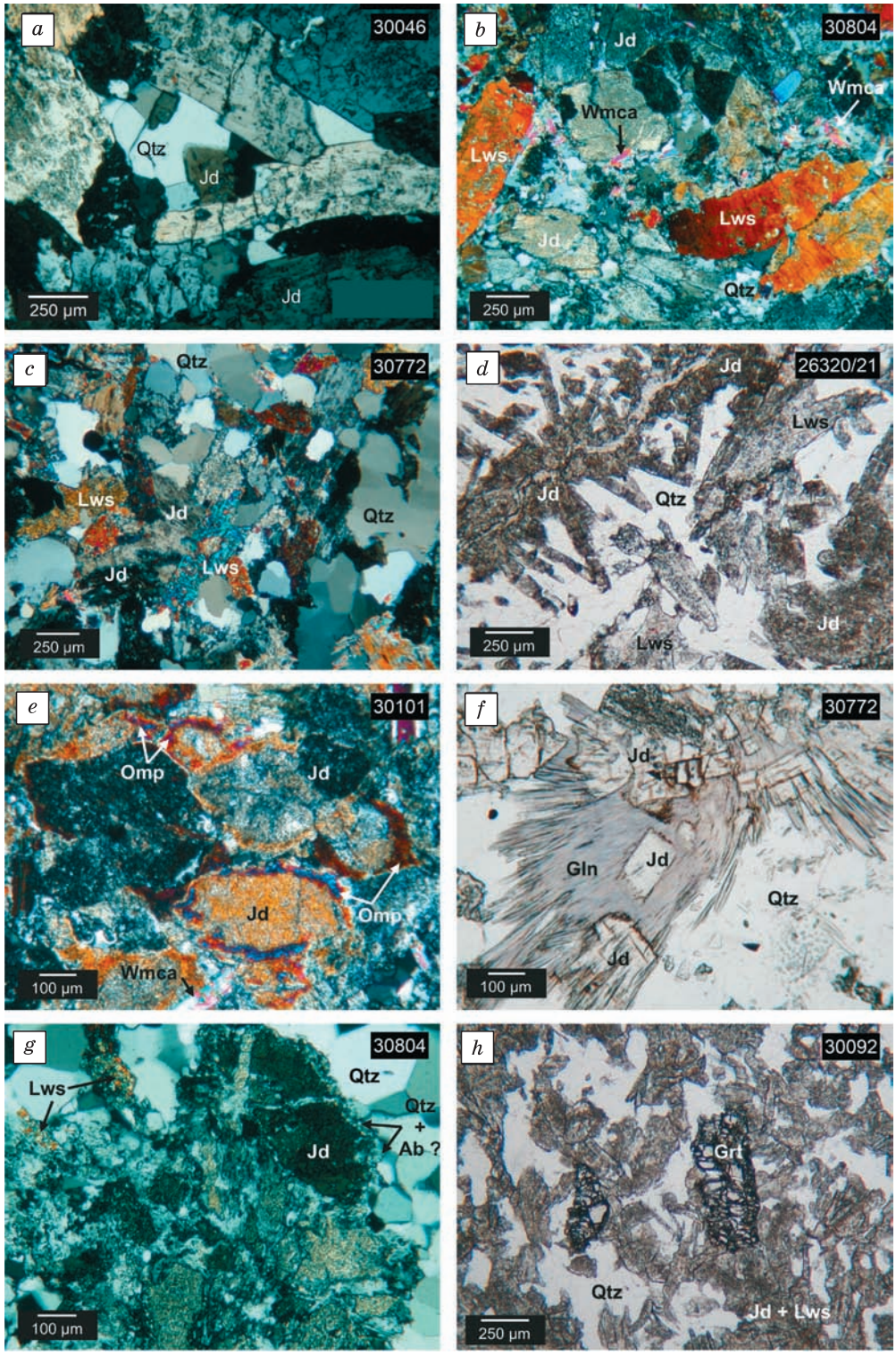

Fig. 6. Microphotographs of thin-sections of matrix-quartz-bearing jadeite rocks (crossed polarizers: *a–c, e, g*; plane-polarized light: *d, f, h*).

a, Subhedral jadeite crystals and interstitial quartz; *b*, anhedral jadeite grains and deformed lawsonite blasts; *c*, subhedral to anhedral jadeite and lawsonite grains; *d*, inclusion-rich subhedral jadeite columns radiating from a small fissure; *e*, jadeite nodules surrounded by omphacite rim; *f*, intergrowth of transparent jadeite and glaucophane; *g*, jadeite grains rimmed by fine-grained albite in quartz matrix; *h*, xenoblastic garnet. Gln, Glaucophane; Grt, garnet; other mineral abbreviations as in Fig. 3.

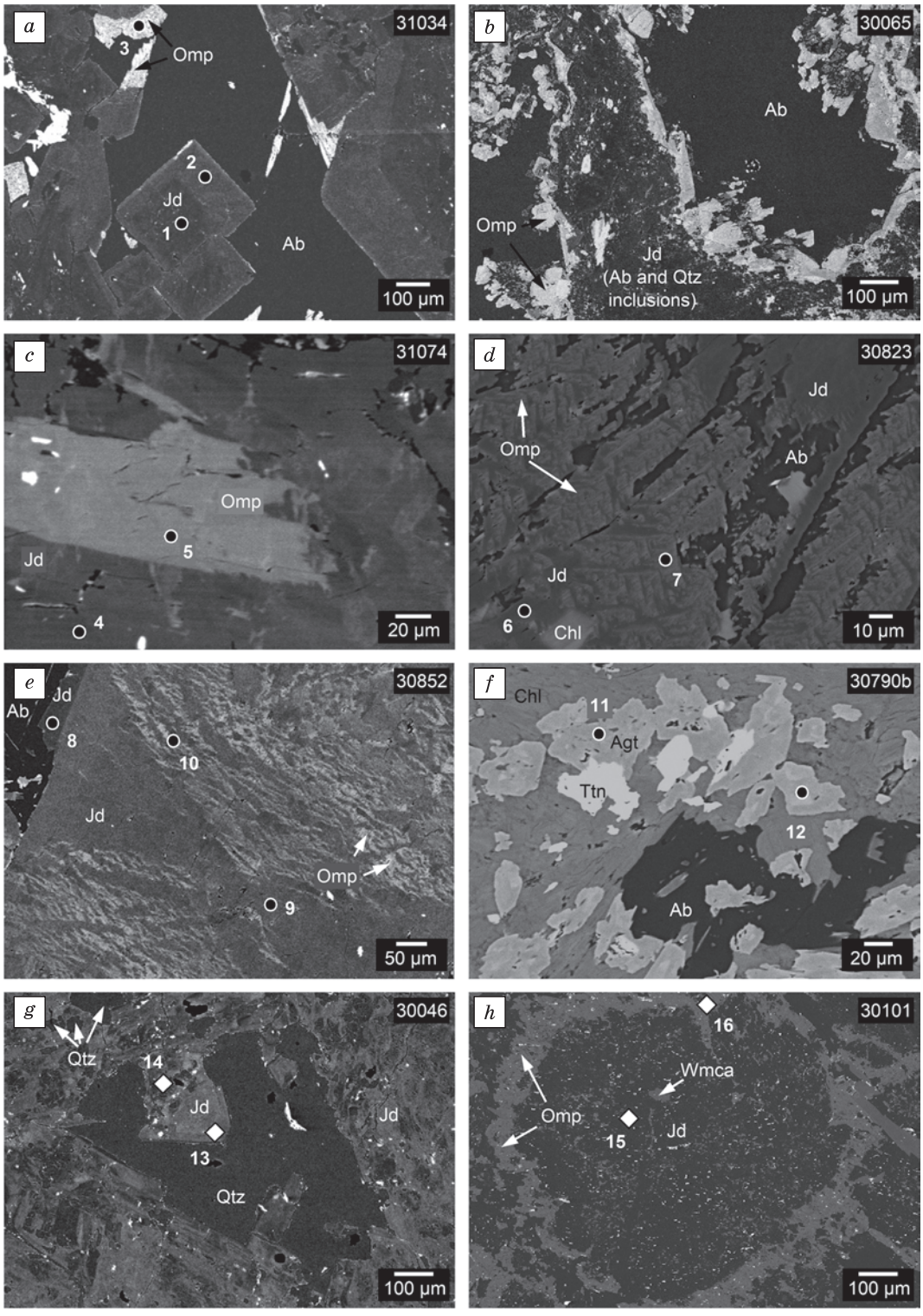

Fig. 7. Back-scattered electron images of clinopyroxenes in matrix-quartz-free (*a–f*) and matrix-quartz-bearing (*g*, *h*) jadeite rocks.

a, *b*, Omphacite overgrowth on jadeite; *c*, omphacite core in jadeite grains; *d*, intergrowth of jadeite, omphacite, and albite; *e*, hourglasslike distribution of omphacite inclusions in jadeite crystal; *f*, rare aegirine-augite; *g*, jadeite and interstitial quartz; *h*, jadeite nodule rimmed by omphacite. For analyses see Fig. 8 and Table 4. Agt, Aegirine-augite; Ttn, titanite; other mineral abbreviations as in Fig. 3.

Table 4. **Chemistry of clinopyroxene**

Number*	1	2	3	4	5	6	7	8	9	10	11	12	13	14	15	16
Sample	31034	31034	31034	31074	31074	30823	30823	30852	30852	30852	30790b	30790b	30046	30046	30101	30101
Rock suite**	f	f	f	f	f	f	f	f	f	f	f	f	b	b	b	b
Abbrev. rock type***	Jdt. s.str.	Jdt. s.str.	Jdt. s.str.	Jdt	Jdt	Jdt	Jdt	Jdt. s.str.	Jdt. s.str.	Jdt. s.str.	Jdr	Jdr	Jdt. s.str.	Jdt. s.str.	dJLQ	dJLQ
SiO_2	58.54	59.45	56.55	58.17	55.31	57.63	55.99	59.18	58.54	56.52	53.02	53.61	57.96	58.45	59.31	55.40
TiO_2	0.24	0.15	0.26	0.15	0.06	0.05	0.13	0.22	0.07	0.09	0.32	0.21	0.04	0.02	0.04	0.01
Al_2O_3	20.29	23.86	10.47	21.60	10.79	20.20	14.57	21.28	19.37	12.11	2.94	2.75	23.54	25.61	25.44	9.48
Cr_2O_3	b.d.l.	0.02	b.d.l.	b.d.l.	b.d.l.	b.d.l.	b.d.l.	0.06	b.d.l.	b.d.l.	b.d.l.	0.06	b.d.l.	b.d.l.	b.d.l.	0.02
FeO	2.89	0.96	3.34	1.93	5.69	3.29	5.10	2.02	4.72	6.38	15.55	15.47	0.37	0.02	0.00	7.15
MgO	2.35	0.93	8.86	1.68	6.82	1.45	4.34	1.91	1.95	5.93	7.03	7.44	1.15	0.01	0.01	6.97
MnO	0.05	0.00	0.13	0.03	0.21	0.00	0.13	0.10	0.06	0.35	0.12	0.28	0.06	0.05	0.01	0.33
CaO	3.32	1.68	13.20	2.46	12.87	2.38	7.64	2.81	3.25	10.10	12.72	14.36	1.88	0.10	0.07	13.16
Na_2O	13.11	14.05	7.40	13.52	7.14	13.59	10.10	13.61	13.10	8.81	6.81	5.90	13.90	15.07	15.27	7.02
K_2O	b.d.l.	0.03	b.d.l.	b.d.l.	0.02	0.02	b.d.l.	b.d.l.	0.02	b.d.l.	0.04	b.d.l.	b.d.l.	b.d.l.	b.d.l.	b.d.l.
Sum	100.81	101.13	100.21	99.53	98.91	98.61	98.01	101.21	101.10	100.30	98.56	100.12	98.91	99.35	100.17	99.62
FeO_{corr}	0.91	0.96	0.70	0.85	4.17	0.23	2.51	0.74	1.55	2.93	3.04	4.93	0.34	0.00	0.00	4.03
$Fe_2O_{3\ corr}$	2.21	–	2.94	1.20	1.69	3.41	2.88	1.43	3.52	3.84	13.90	11.71	0.03	0.02	–	3.47
$\sum_{corr}$	101.03	101.13	100.50	99.65	99.08	98.95	98.30	101.35	101.45	100.69	99.96	101.29	98.91	99.35	100.17	99.91
Si	1.99	2.00	1.99	1.99	2.00	2.00	2.00	2.00	2.00	2.00	1.98	1.98	1.99	1.98	1.99	2.00
$Al^{[IV]}$	0.01	0.00	0.01	0.01	0.00	0.00	0.00	0.00	0.00	0.00	0.02	0.02	0.01	0.02	0.01	0.00
$\sum_T$	2.00	2.00	2.00	2.00	2.00	2.00	2.00	2.00	2.00	2.00	2.00	2.00	2.00	2.00	2.00	2.00
Al	0.80	0.94	0.42	0.87	0.46	0.82	0.61	0.84	0.78	0.50	0.11	0.10	0.94	1.00	1.00	0.40
Fe^{3+}	0.06	–	0.08	0.03	0.05	0.09	0.08	0.04	0.09	0.10	0.39	0.33	0.00	0.00	–	0.09
Ti	0.01	0.00	0.01	0.00	0.00	0.00	0.00	0.01	0.00	0.00	0.01	0.01	0.00	0.00	0.00	0.00
Mg	0.12	0.05	0.46	0.09	0.37	0.08	0.23	0.10	0.10	0.31	0.39	0.41	0.06	0.00	0.00	0.37
Fe^{2+}	0.01	0.01	0.02	0.01	0.13	0.01	0.07	0.02	0.03	0.08	0.09	0.15	0.00	0.00	0.00	0.12
$\sum_{M1}$	1.00	1.00	0.99	1.00	1.00	1.00	1.00	1.00	1.00	1.00	0.99	1.00	1.00	1.00	1.00	0.99
Mg	0.00	0.00	0.00	0.00	0.00	0.00	0.00	0.00	0.00	0.00	0.00	0.00	0.00	0.00	0.00	0.00
Fe^{2+}	0.01	0.02	0.00	0.01	0.00	0.00	0.00	0.00	0.01	0.00	0.00	0.00	0.01	0.00	0.00	0.00
Ca	0.12	0.06	0.50	0.09	0.50	0.09	0.29	0.10	0.12	0.38	0.51	0.57	0.07	0.00	0.00	0.51
Na	0.86	0.92	0.50	0.90	0.50	0.91	0.70	0.89	0.87	0.60	0.49	0.42	0.92	0.99	1.00	0.49
$\sum_{M2}$	1.00	1.00	1.00	1.00	1.00	1.00	0.99	1.00	1.00	0.99	1.00	0.99	1.00	0.99	1.00	1.00
Jd (mol.%)	80.8	91.6	42.6	86.7	45.4	82.5	62.2	85.4	77.6	50.1	10.6	10.1	92.2	99.0	99.5	39.7
Ae	5.7	0.0	7.8	3.1	4.6	8.9	7.8	3.7	9.0	10.2	38.6	32.2	0.1	0.0	0.0	9.4
Di	11.1	5.3	47.5	7.9	37.2	7.9	22.6	9.0	9.2	31.0	40.8	42.1	6.6	1.0	0.5	38.4
Hed	2.4	3.1	2.1	2.3	12.8	0.7	7.3	1.9	4.1	8.6	9.9	15.6	1.1	0.0	0.0	12.5

* See Fig. 7 for location of analyses.

** b, matrix-quartz-bearing suite; f, matrix-quartz-free suite.

*** See Table 1.

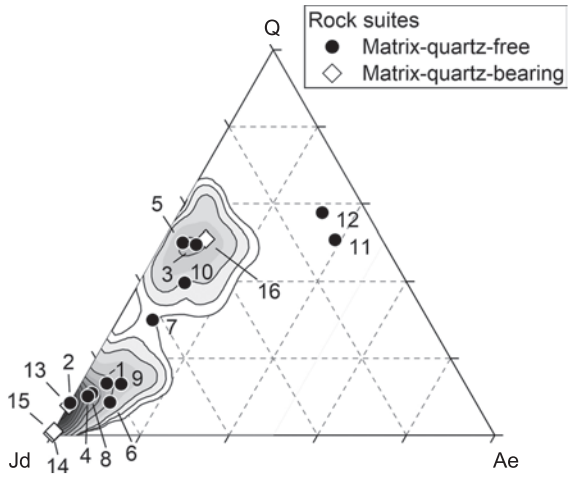

Fig. 8. Ternary diagram after Morimoto et al. (1988) of the clinopyroxene analyses presented in Fig. 7 and Table 4.

Contours show the density distribution of all the clinopyroxene analyses from the samples of this study; darker shading represents higher numbers of analyses with this particular composition. Jd, Jadeite; Q, calcium–iron–magnesium pyroxenes (Quad); Ae, aegirine.

MgO contents (46 < SiO_2 < 61 wt.%; MgO up to 6 wt.%) when compared to the matrix-quartz-bearing rocks (60 < SiO_2 < 75 wt.%; MgO < 1.5 wt.%). The Al_2O_3, CaO, and Fe_2O_{3Tot} contents of both rock suites are usually below 24, 9, and 7 wt.%, respectively (Table 5). In general, the jadeite rocks have low MnO (<0.1 wt.%) and moderately high TiO_2 (<1 wt.%) contents. The matrix-quartz-free jadeite rocks can further be subdivided into two chemical subgroups: group I, comprising *jadeitite s.str.* and albite-rich jadeite rocks with low modal amounts of omphacite, chlorite, and epidote-supergroup minerals, show high Na_2O (<10 wt.%) and low MgO contents (<3 wt.%); group II, comprising chlorite- and epidote-supergroup-bearing jadeite rocks, as well as omphacite-rich rocks, is characterized by lower Na_2O contents and higher concentrations of MgO, CaO, Fe_2O_{3Tot}, MnO, and TiO_2.

Trace-element analyses of rocks from both suites show that Rb and Ba concentrations correlate with K_2O contents, indicating the presence of white mica in these rocks. Zirconium contents are highest in SiO_2-poor rocks (up to 300 ppm); the lowest Zr content is found in one of the discordant jadeite–lawsonite quartzites (<2 ppm, sample 30105). The overall REE content is inversely correlated with SiO_2 and positively correlated with Fe_2O_{3Tot}

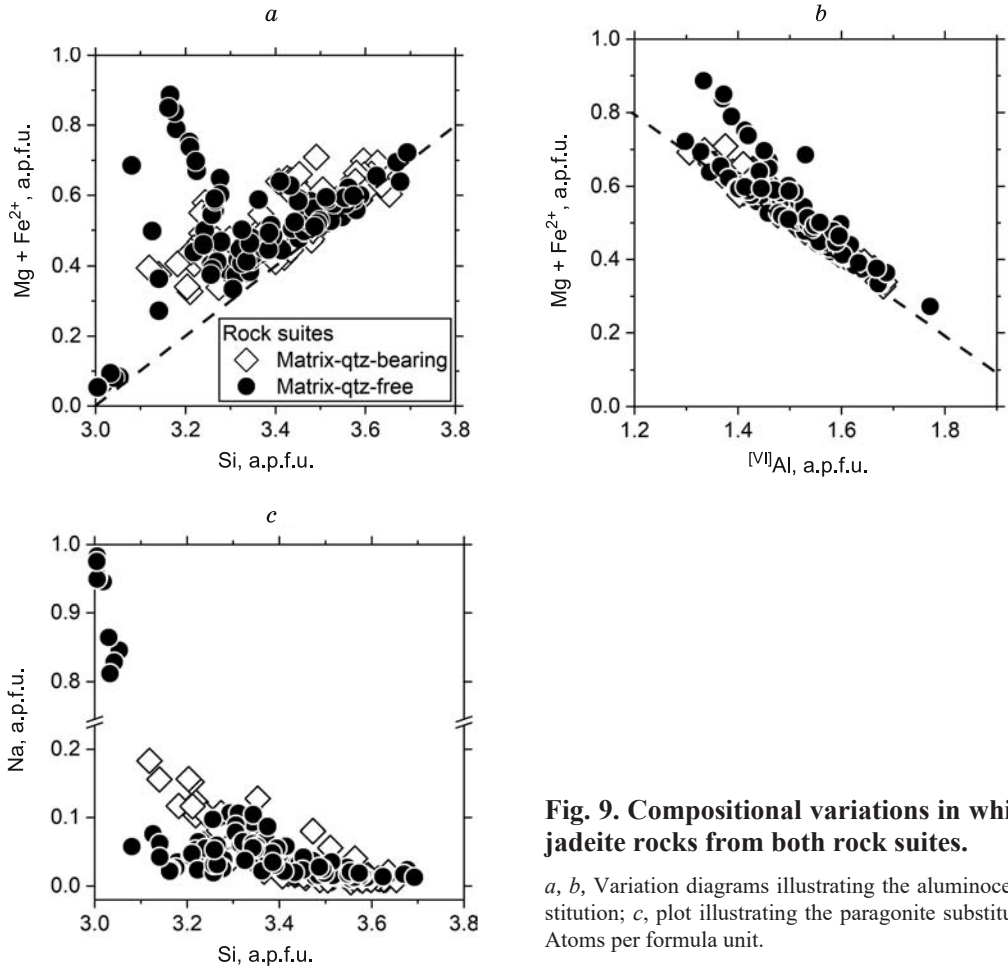

Fig. 9. Compositional variations in white mica of jadeite rocks from both rock suites.

a, *b*, Variation diagrams illustrating the aluminoceladonite substitution; *c*, plot illustrating the paragonite substitution. a.p.f.u., Atoms per formula unit.

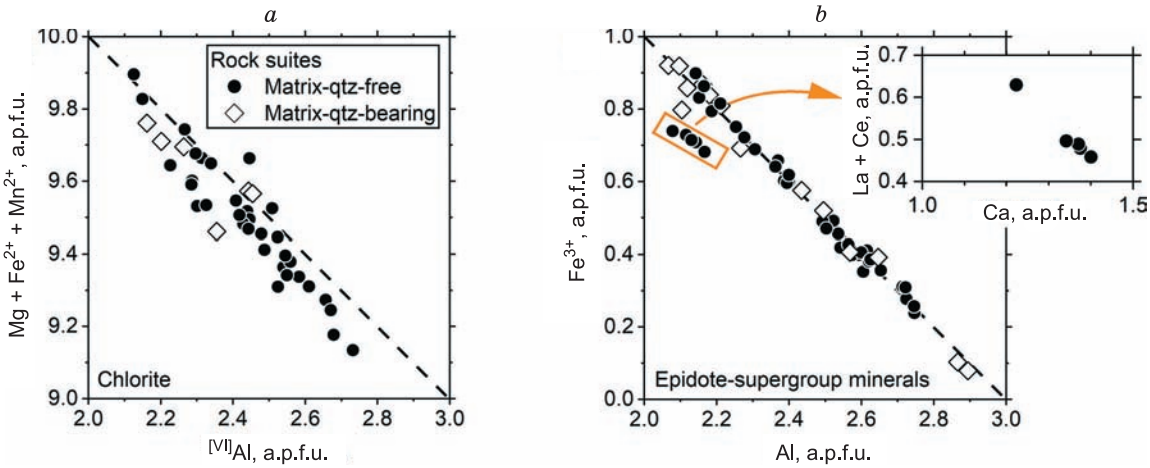

Fig. 10. Compositional variations in (*a*) chlorite and (*b*) epidote-supergroup minerals of jadeite rocks from both rock suites. a.p.f.u., Atoms per formula unit.

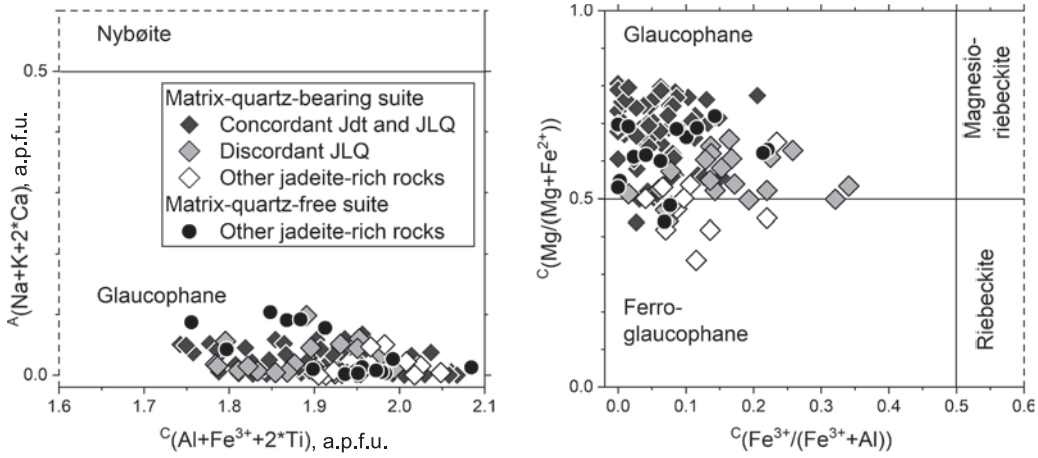

Fig. 11. Compositional variations in glaucophane of jadeite rocks from both rock suites. Amphibole classification of Hawthorne et al. (2012). a.p.f.u., Atoms per formula unit.

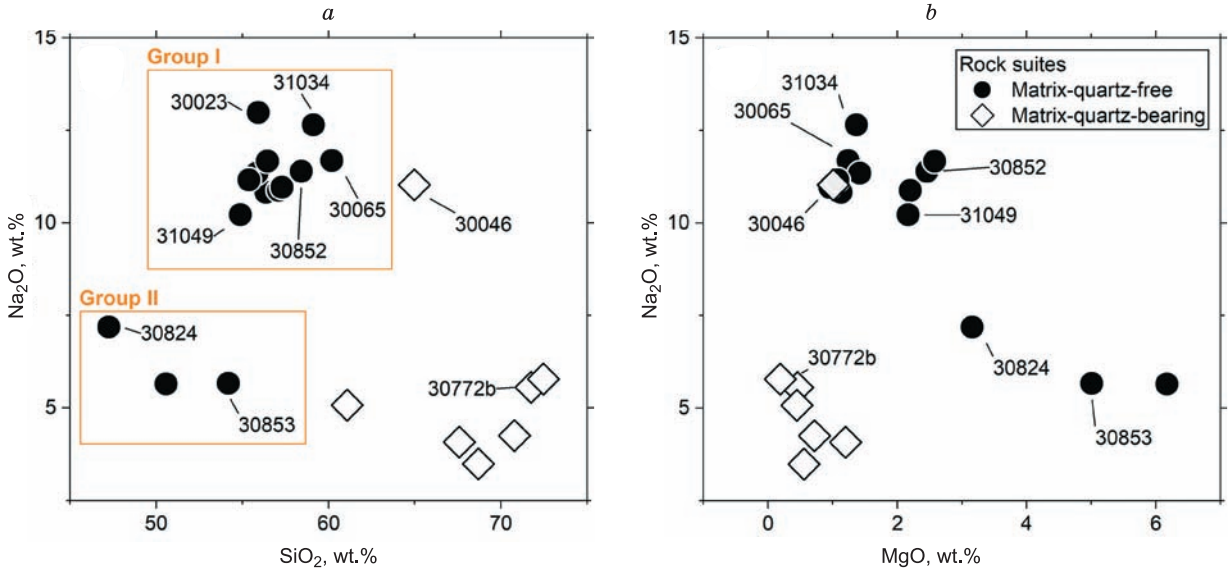

Fig. 12. Variation diagrams of Na_2O, SiO_2, and MgO for the matrix-quartz-free and -bearing samples of this study. Isocon analysis (Fig. 14) was performed on the labeled samples. Two chemical groups are outlined.

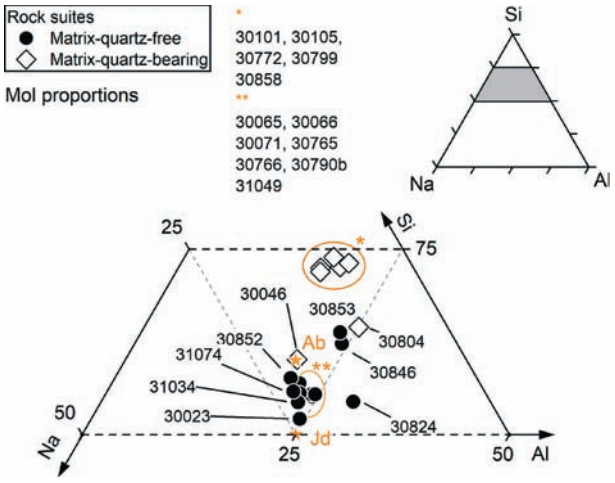

Fig. 13. Triangular plots showing the molar proportions of Na, Si, and Al for matrix-quartz-free and -bearing samples. Diagram modified after Coleman (1961).

and Zr concentrations. Jadeite rocks with elevated concentrations of P_2O_5 also tend to possess higher overall REE contents, pointing to apatite-group minerals as the dominant REE host mineral in these samples.

Figure 13 shows a triangular diagram similar to that developed by Coleman (1961) to illustrate the chemical variations in the Clear Creek jadeitites. The plotted molar proportions of Na, Si, and Al can, in principle, be used to estimate the (molar) abundances of jadeite, albite, and quartz in jadeite rocks. However, even for an almost pure *jadeitite s.str.* (e.g., sample 31034), this chemography indicates a high relative molar abundance of albite to jadeite (albite:jadeite ≈ 40:60), which might be due to the omphacite component of the jadeitic clinopyroxene that is left unconsidered in this graphical representation of the whole-rock geochemistry. As pointed out by Coleman (1961), jadeite rocks should have Na/Al ≈ 1, which is consistent with analyses of most jadeitites of this study but not with group-II jadeite rocks of the matrix-quartz-free suite (e.g., samples 30824 and 30846) and lawsonite-rich samples from the matrix-quartz-bearing rock suite (e.g., sample 30804).

DISCUSSION

The majority of jadeitites worldwide are interpreted to be of P-type origin; i.e., they are expected to have formed by direct crystallization from a high-pressure fluid, a conclusion based mainly on a combination of three arguments (Harlow et al., 2014). First, the replacement of an igneous protolith, whether felsic or mafic, would involve a prohibitively complex mass transfer between metasomatizing fluid and the protolith. Second, with a few exceptions, relict igneous textures are generally not found in jadeitites, and potential precursor rocks unaffected by metasomatism are usually not documented in the block inventory of serpentinite-matrix mélanges. Third, there is abundant evidence for the presence of fluids during jadeitite genesis, as attested to, for instance, by rhythmical or oscillatory zoning patterns typical of open-system crystallization and fluid inclusions in jadeite. The discordant matrix-quartz-bearing veins found in some blueschists with their crack-seal characteristics must clearly be P-type. For other samples, the evidence must be critically evaluated. Previous studies in the RSJC (Hertwig, 2014; Hertwig et al., 2016) led to the view that plagiogranite might represent a logical precursor rock type for the RSJC jadeite-rich rocks, suggesting that they are R-type. In the following, we will therefore briefly consider the most important features of oceanic plagiogranites and then explore in more detail the possibility that certain jadeite rocks from the RSJC might have formed by metasomatic replacement of an igneous precursor rock by separately addressing each of the three above-mentioned arguments.

Oceanic plagiogranites and their connection with jadeite–lawsonite quartzites, jadeite quartzites, and lawsonite quartzites

In a metasomatic-replacement (R-type) scenario, a plausible precursor rock for jadeitites is oceanic plagiogranite, a term proposed for a "plutonic rock consisting of oligoclase or andesine, quartz and less than 10% of biotite and hornblende. May be used as a synonym for trondhjemite and leucocratic tonalite [...]" (Recommendation of the IUGS Subcommission on the Systematics of Igneous Rocks (Le Maitre, 2002, p. 130)). Initially recognized in ophiolite complexes worldwide (Coleman, 1977; Koepke et al., 2004, 2007, for a list of occurrences), plagiogranites, or "felsic veins," have also been described in modern oceanic lithosphere (Aldiss, 1981; Niu et al., 2002; Schwartz et al., 2010), where they range from small veinlets to meter-sized dikes and veins and irregular-shaped bodies (Koepke et al., 2007). In detail, this suite of leucocratic rocks can be highly variable and include diorite as well as tonalite and trondhjemite. These rocks occur in "small, but ubiquitous [amounts]" in the gabbroic section of the crust (Koepke et al., 2004). Therefore, in principle, oceanic plagiogranites are available to serve as precursor rocks for jadeitites. Furthermore, high-pressure analogs of oceanic plagiogranites that escaped metasomatism are an expected, though minor, component of the block inventory of serpentinite-matrix mélanges.

Table 5. **Major- and trace-element whole-rock geochemistry of jadeite rocks from the RSJC**

Sample	30023	30046	30065	30066	30071	30101	30105	30765	30766	30772	30790b	30799	30804	30824	30846	30852	30853	30858	31034	31049	31074
Rock suite*	f	b	f	f	f	b	b	f	f	b	f	b	b	f	f	f	f	b	f	f	f
Abbrev. rock type**	Jdt s.str.	Jdt s.str.	Jdt	Jdt	Jdt	dJLQ	dJLQ	Jdr	Jdr	JLQ	Jdr	JLQ	JLQ	Jdt	Jdr	Jdt s.str.	Jdr	LQ	Jdt s.str.	Jdt s.str.	Jdt
Method ***	m1/t1	m1/t2	m1/t1	m1/t1	m1/t1	m1/t2	m1/t2	m1/t2	m1/t2	m1/t2	m1/t2	m1/t1	m1/t1	m1/t2	m1/t2	m1/t2	m1/t2	m1/t2	m1/t2	m1/t1	m1/t2
wt.%																					
1	2	3	4	5	6	7	8	9	10	11	12	13	14	15	16	17	18	19	20	21	22
SiO_2	55.92	64.98	60.18	56.36	55.84	67.58	68.70	57.09	57.29	71.75	55.39	70.79	61.08	47.25	50.58	58.41	54.19	72.47	59.11	54.88	56.45
TiO_2	0.30	0.16	0.13	0.27	0.46	0.05	0.04	0.31	0.37	0.12	0.36	0.24	0.30	0.77	1.45	0.50	0.49	0.10	0.42	0.53	0.42
Al_2O_3	22.22	18.44	19.65	21.18	19.66	14.94	15.69	21.08	18.80	14.04	19.19	14.23	20.21	21.76	16.73	17.74	16.81	14.48	21.32	20.66	18.71
Fe_2O_{3Tot}	1.32	0.87	1.28	1.95	3.32	1.53	0.81	2.65	2.44	1.24	1.92	2.00	1.49	7.06	4.17	4.88	5.00	0.93	1.33	3.22	3.05
CaO	3.65	1.34	3.26	3.20	5.72	6.63	6.49	2.74	4.71	3.34	5.96	3.59	5.96	7.35	8.66	3.79	5.74	2.45	2.14	3.17	4.34
MgO	<0.02	1.01	1.24	1.13	1.42	1.20	0.56	2.20	0.96	0.46	1.08	0.72	0.45	3.16	6.17	2.46	5.01	0.19	1.37	2.17	2.58
MnO	0.03	0.03	0.03	0.03	0.06	0.09	0.04	0.04	0.03	0.03	0.04	0.04	0.02	0.10	0.09	0.16	0.08	0.02	0.03	0.04	0.05
K_2O	0.19	0.03	0.29	1.90	0.35	0.15	0.16	1.33	0.05	0.18	0.07	0.76	0.81	0.15	2.06	0.14	4.09	0.48	0.04	1.48	0.07
Na_2O	12.98	11.03	11.68	10.83	11.34	4.08	3.49	10.88	10.96	5.56	11.16	4.25	5.08	7.19	5.65	11.39	5.67	5.78	12.65	10.22	11.67
P_2O_5	0.13	0.05	<0.01	0.12	0.10	0.01	0.13	0.10	0.09	<0.01	0.10	0.03	0.09	0.16	0.53	<0.01	0.05	0.02	0.01	0.12	<0.01
Sum	96.74	97.94	97.74	96.97	98.27	96.26	96.11	98.42	95.70	96.72	95.27	96.65	95.49	94.95	96.09	99.47	97.13	96.92	98.42	96.49	97.34
H_2O	1.46	0.55	1.10	1.41	1.01	3.74	3.46	0.22	<0.01	1.44	0.83	2.28	3.84	4.98	2.38	1.22	2.6	1.5	0.28	1.98	1.01
CO_2	1.53	0.08	0.35	0.54	0.09	0.07	0.01	0.19	2.64	0.10	3.84	0.10	0.08	0.10	0.10	0.08	0.09	0.15	0.58	0.03	0.53
FeO	0.34	0.30	0.42	0.56	1.13	0.63	0.36	0.56	0.67	0.23	0.64	0.79	0.32	3.28	2.55	0.85	1.21	0.58	0.25	0.73	0.54
Fe_2O_3	0.94	0.54	0.81	1.33	2.06	0.83	0.41	2.03	1.70	0.99	1.21	1.12	1.14	3.42	1.33	3.94	3.66	0.28	1.05	2.41	2.45
ppm																					
Li	N.A.	N.A.	N.A.	N.A.	N.A.	N.A.	N.A.	22	<17	<17	18	N.A.	N.A.	40	50	35	20	<17	N.A.	N.A.	N.A.
Cd	10	5	11	14	11	6	6	8	7	6	7	5	8	7	8	6	8	<5	<5	9	6
Cl	66	<31	59	71	53	<31	<31	<31	<31	<31	<31	<31	<31	<31	<31	<31	<31	<31	34	<31	75
Cr	14	<6	19	39	31	6	<6	9	<6	<6	<6	<6	<6	13	118	31	118	<6	10	16	31
Cu	2	<4	1	16	4	7	13	8	8	8	53	60	15	16	47	<4	46	<4	<4	27	<4
F	<247	<247	<247	<247	<247	<247	<247	<247	<247	<247	<247	<247	<247	461	<247	<247	<247	<247	<247	<247	<247
Mo	<2	3	3	3	2	3	3	3	3	3	2	3	<2	<2	3	4	2	3	6	7	4
Ni	14	18	31	42	27	17	13	27	3	4	<3	5	3	12	129	31	103	10	28	16	47
Pb	<6	<6	<6	<6	<6	<6	<6	<6	<6	<6	8	<6	<6	<6	<6	<6	<6	<6	<6	<6	<6
S	<21	<21	<21	<21	<21	<21	<21	<21	1381	46	<21	375	87	<21	<21	<21	<21	302	<21	<21	<21
Sb	<11	12	18	17	11	<11	12	<11	<11	14	<11	<11	<11	26	20	14	13	<11	11	<11	10

Table 5 (*continued*)

1	2	3	4	5	6	7	8	9	10	11	12	13	14	15	16	17	18	19	20	21	22
Zn	22	17	23	26	35	17	20	24	19	17	19	14	20	25	16	22	17	18	18	16	18
Ba	92	12	278	1692	225	71	80	616	20	52	32	391	402	85	1325	103	1871	195	31	1220	111
Be	N.A.	<1	N.A.	N.A.	N.A.	1	<1	<1	<1	<1	1	N.A.	N.A.	<1	<1	1	<1	<1	<1	N.A.	<1
Co	N.A.	75.5	N.A.	N.A.	N.A.	83.1	60.4	55.7	26.3	62.8	29.3	N.A.	N.A.	36.3	33.4	39.7	28.8	37.7	92.3	N.A.	101.1
Cs	N.A.	<0.1	N.A.	N.A.	N.A.	<0.1	<0.1	0.3	<0.1	<0.1	<0.1	N.A.	N.A.	<0.1	0.5	0.4	0.7	<0.1	<0.1	N.A.	0.1
Ga	N.A.	7.3	N.A.	N.A.	N.A.	9.2	7.2	13.2	10.8	9.7	10.6	N.A.	N.A.	15.5	15.3	11.6	13.2	10	12.1	N.A.	13.9
Hf	N.A.	0.9	N.A.	N.A.	N.A.	1	<0.1	1.5	2.8	1.7	3.1	N.A.	N.A.	4.9	7.2	7	1.9	2.2	4.4	N.A.	3.1
Nb	1	0.6	<1	4	6	<0.1	<0.1	0.7	0.8	0.4	1	3	6	0.7	16.7	5.2	2.2	<0.1	9.1	5	1.8
Rb	2	0.4	5	47	7	1.9	2	26.7	0.7	2.9	0.8	15	15	2.3	40.4	5.4	87.8	8.7	<0.1	35	1.7
Sn	N.A.	<1	N.A.	N.A.	N.A.	<1	<1	<1	<1	<1	<1	N.A.	N.A.	<1	2	2	<1	<1	<1	N.A.	<1
Sr	572	23.6	101	233	268	141.8	173.4	36.1	401.2	200.2	578.9	244	935	944.1	308.1	69	40.6	295.2	80.2	90	71.5
Ta	N.A.	1.5	N.A.	N.A.	N.A.	1.3	0.8	1.3	0.3	1.2	0.7	N.A.	N.A.	0.4	0.9	0.9	0.4	0.5	1.8	N.A.	1.3
Th	N.A.	<0.2	N.A.	N.A.	N.A.	<0.2	<0.2	<0.2	<0.2	0.3	<0.2	N.A.	N.A.	<0.2	0.2	3	0.5	<0.2	<0.2	N.A.	2.4
U	N.A.	<0.1	N.A.	N.A.	N.A.	<0.1	<0.1	<0.1	<0.1	<0.1	<0.1	N.A.	N.A.	0.1	0.3	1.5	0.4	<0.1	0.1	N.A.	0.6
V	N.A.	15	N.A.	N.A.	N.A.	44	29	49	29	12	23	N.A.	N.A.	48	95	99	117	<8	17	N.A.	44
W	N.A.	809.1	N.A.	N.A.	N.A.	926.1	662.6	627.6	238.6	849	348.8	N.A.	N.A.	230.2	116.6	360.6	137.2	402.9	865.7	N.A.	777.5
Zr	121	28.4	25	87	123	37.7	1.8	63.1	126.3	77	130.4	65	171	180.6	292.9	254.3	74.9	81	195.1	179	145.4
Y	2	1.2	2	7	8	3.3	2.6	5.8	3.2	3.4	3.3	5	<1	22	25.3	35.5	10.9	3.6	3.1	11	7.6
La	N.A.	3.7	N.A.	N.A.	N.A.	0.4	0.4	1.8	2	3.4	2.4	N.A.	N.A.	2.9	8.5	16.3	3.8	2.3	1.2	N.A.	14.2
Ce	N.A.	4.4	N.A.	N.A.	N.A.	0.7	0.6	3.1	3.1	5.1	4.2	N.A.	N.A.	6.8	20.2	27	7.8	4.4	3.2	N.A.	25.5
Pr	N.A.	0.46	N.A.	N.A.	N.A.	0.11	0.11	0.51	0.49	0.55	0.58	N.A.	N.A.	1.42	3.94	3.63	1.16	0.45	0.65	N.A.	2.92
Nd	N.A.	1.5	N.A.	N.A.	N.A.	0.5	0.8	2.6	2.6	2.3	3.2	N.A.	N.A.	9.8	21.6	16.6	5.5	2.3	2.4	N.A.	10.4
Sm	N.A.	0.21	N.A.	N.A.	N.A.	0.2	0.17	0.91	0.49	0.16	0.53	N.A.	N.A.	3	5.23	4.58	1.48	0.41	0.7	N.A.	1.75
Eu	N.A.	0.21	N.A.	N.A.	N.A.	0.09	0.1	0.38	0.44	0.25	0.39	N.A.	N.A.	1.14	1.9	1.22	0.53	0.42	0.5	N.A.	0.65
Gd	N.A.	0.16	N.A.	N.A.	N.A.	0.25	0.28	0.97	0.55	0.29	0.47	N.A.	N.A.	3.48	5.3	5.11	1.8	0.35	0.59	N.A.	1.56
Tb	N.A.	0.01	N.A.	N.A.	N.A.	0.04	0.04	0.15	0.09	0.05	0.07	N.A.	N.A.	0.57	0.77	0.92	0.27	0.05	0.06	N.A.	0.24
Dy	N.A.	0.32	N.A.	N.A.	N.A.	0.43	0.37	0.97	0.49	0.41	0.67	N.A.	N.A.	4.04	4.97	6.01	2.3	0.57	0.59	N.A.	1.46
Ho	N.A.	0.04	N.A.	N.A.	N.A.	0.08	0.07	0.21	0.09	0.1	0.11	N.A.	N.A.	0.77	0.87	1.21	0.41	0.07	0.1	N.A.	0.25
Er	N.A.	0.12	N.A.	N.A.	N.A.	0.47	0.24	0.59	0.39	0.21	0.43	N.A.	N.A.	2.43	2.35	3.91	1.16	0.41	0.32	N.A.	0.7
Tm	N.A.	<0.01	N.A.	N.A.	N.A.	0.05	0.02	0.09	0.05	0.04	0.06	N.A.	N.A.	0.32	0.37	0.62	0.19	0.06	0.04	N.A.	0.12
Yb	N.A.	0.15	N.A.	N.A.	N.A.	0.29	0.24	0.65	0.48	0.45	0.54	N.A.	N.A.	2.28	2.14	4.44	1.28	0.46	0.5	N.A.	0.74
Lu	N.A.	0.03	N.A.	N.A.	N.A.	0.05	0.01	0.07	0.07	0.06	0.07	N.A.	N.A.	0.37	0.36	0.65	0.21	0.09	0.07	N.A.	0.11

* b, matrix-quartz-bearing suite; f, matrix-quartz-free suite.

** See Table 1.

*** See “Analytical Methods” for details on analytical procedures.

Table 6. **Plagiogranite compositions used for isocon analysis in Fig. 14**

wt.%	Plagiogranite of composition 30772 JLQ	Newfoundland, plutonic, SSZ-O (Malpas, 1979)	MAR, subvolcanic, MOR (Aumento, 1969)	Chile, plutonic, SSZ-O (Saunders et al., 1979)
SiO_2	71.75	60.25	61.97	65.51
TiO_2	0.12	0.54	0.94	0.81
Al_2O_3	14.04	18.05	16.00	13.64
Fe_2O_{3Tot}	1.24	2.75	7.19	6.55
CaO	3.34	5.71	3.24	6.28
MgO	0.46	1.49	2.43	1.46
MnO	0.03	0.03	0.09	0.11
K_2O	0.18	0.05	0.75	0.67
Na_2O	5.56	8.26	5.55	1.99
P_2O_5	b.d.l.	0.17	0.22	0.17
Sum	96.72	97.30	98.38	97.19

Thermodynamic calculations demonstrate that an oceanic plagiogranite of trondhjemitic to tonalitic whole-rock chemistry should be transformed into a jadeite- and lawsonite-rich quartzite when subjected to blueschist-facies metamorphic conditions during subduction (Hertwig, 2014). The normative amounts of albite and anorthite in the protolith govern the proportions of jadeite and lawsonite in the metamorphic rock. Based on CIPW-normative mineral abundances and the classification diagram for plutonic rocks of O'Connor (1965), trondhjemites and tonalites are potential igneous protoliths for samples 30772(b), 30799, 30804, and 30858 of the matrix-quartz-bearing rock suite. For example, the concordant jadeite–lawsonite quartzite layers of sample 30772 (Fig. 2*f*) possess (in mol.%) normative quartz (32), albite (47), anorthite (13), orthoclase (1), and diopside (2); the protolith of these layers would be trondhjemitic in composition and would transform isochemically into a jadeite–lawsonite quartzite at $P > \sim 1–1.2$ GPa and $T > \sim 350$ °C (Hertwig, 2014). Therefore, based on similarities in whole-rock, major-element compositions, we suggest that jadeite–lawsonite quartzites (disregarding here the P-type discordant varieties), jadeite quartzites, and lawsonite quartzites from the RSJC are products of an isochemical HP/LT metamorphic overprint of oceanic plagiogranites. This might represent one endmember scenario of the R-type genesis of jadeite rocks.

Mass transfer during metasomatic replacement of oceanic plagiogranite: isocon analysis

While oceanic plagiogranites are the logical choice as protoliths of most jadeite–lawsonite quartzites, there is no igneous or sedimentary rock that possesses the whole-rock, major-element composition of the virtually monomineralic jadeitites. By comparing the chemical compositions of a selection of jadeitites with those of possible igneous and sedimentary protoliths, Harlow (1994) showed that, in general, a relatively strong enrichment in Na_2O and Al_2O_3 and loss of predominantly SiO_2 are necessary to obtain the chemical composition of the jadeitites from those of the assumed precursor rocks. For instance, in the particular example of jadeitite TD-1 (Guatemala (Silva, 1970)) and plagiogranite OM-32 (trondhjemitic oceanic plagiogranite, Semail ophiolite, Oman (Coleman and Donato, 1979)), Na_2O and Al_2O_3 show relative increases by a factor of 2.4 and 1.7, respectively, and a decrease by a factor of 0.85 in SiO_2. In addition, there is a loss of FeO_{Tot} and CaO and an increase in the MgO content (Harlow, 1994). These modifications seem to imply an almost prohibitively complex mass balance that needs to be satisfied to metasomatically replace a typical plagiogranite by a jadeitite (Harlow, 1994; Harlow et al., 2014).

We can explore this argument more precisely by investigating the mass balance involved in the formation of the widely acknowledged R-type jadeitite from the Monviso metaophiolite, Western Alps (Compagnoni et al., 2012). The Monviso jadeitite forms the rim around a core of quartz–jadeite rock, with the latter possessing the whole-rock, major- and trace-element compositions of plagiogranites exposed at other locations in the Monviso ophiolite. This relationship strongly indicates that an (oceanic) plagiogranite is the protolith for the quartz–jadeite rock (Compagnoni et al., 2012); the jadeitite rim is then the product of the metasomatic replacement of the original plagiogranite or the quartz–jadeite rock itself. As protolith and metasomatic rind are part of the same tectonic block, there is no ambiguity in matching precursor rock and jadeitite, making it a worthwhile exercise to further explore the mass transfer related to the genesis of this particular jadeitite.

Judging from the whole-rock geochemical data on the jadeitite and quartz–jadeite rock (Compagnoni et al., 2012), Na_2O and Al_2O_3 are enriched by a factor of 1.6 and 1.5, respectively, whereas SiO_2 decreased by a

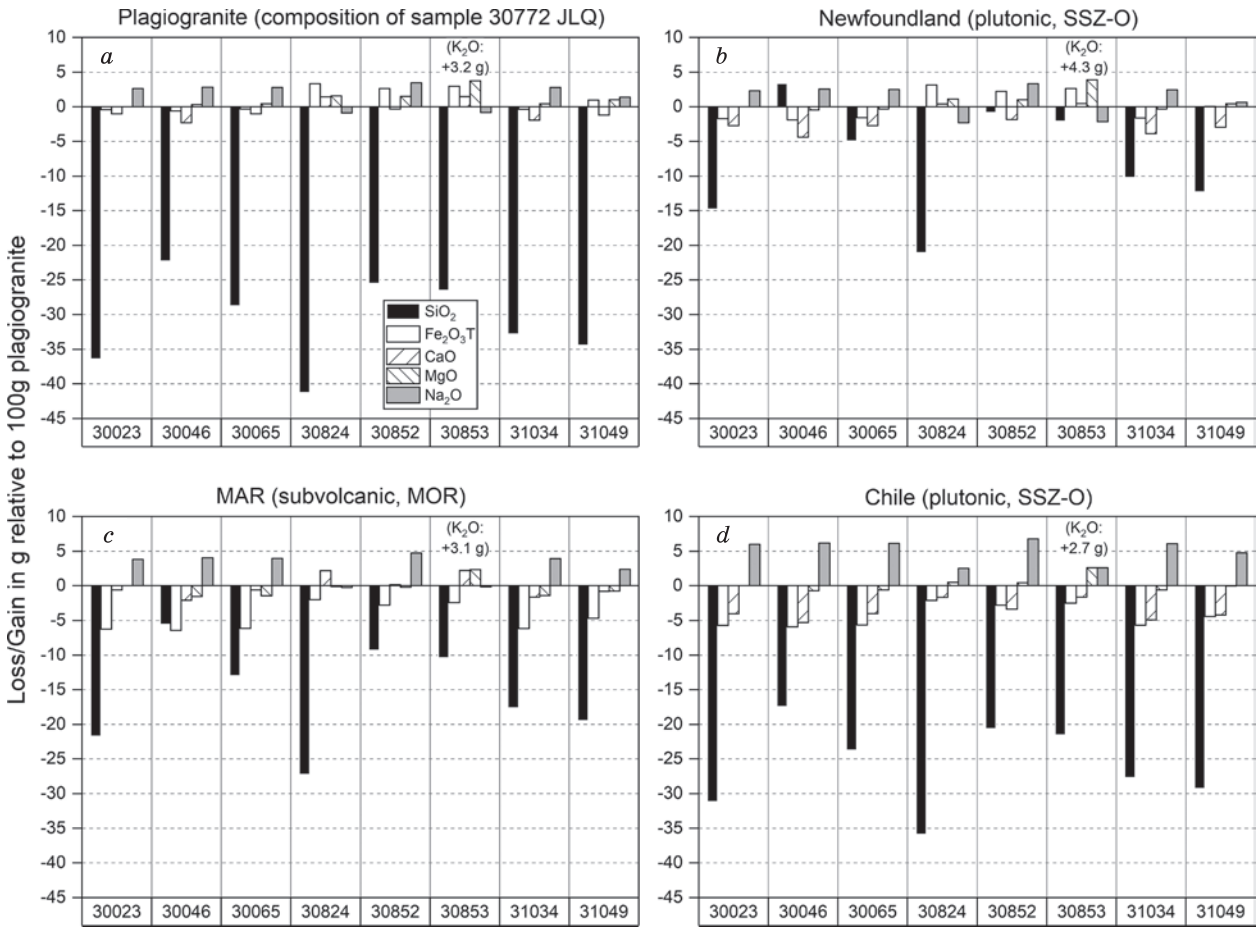

Fig. 14. Bar diagrams illustrating the results of isocon analysis. Negative values indicate that mass was lost during metasomatism, while positive values indicate mass gains.

The order of oxides in the legend and in the bar charts (seen from left to right) is the same. For detailed values see Appendix EA3; for plagiogranite compositions and references see Table 6.

factor of 0.8 during jadeitite genesis. These changes in major-element contents are broadly comparable to the values given by Harlow (1994) for the potential metasomatic formation of the TD-1 jadeitite. However, for estimating the actual amount of mass that had to be transferred to produce the Monviso jadeitite, these factor values are of limited significance; at the same time, the so-called *isocon analysis*, made known to the broader scientific community by Grant (1986, 2005), allows the mass transfer during metasomatism to be quantitatively investigated. An excellent application to jadeitite was presented by Shigeno et al. (2012). By choosing species (oxides) that are assumed to be immobile during metasomatism, it is possible to calculate the mass that is lost from or gained by the protolith during the process. To simplify analysis, we choose Al_2O_3 to be the immobile component that completely remains in its original location (i.e., in the protolith). Assuming 100 g quartz–jadeite rock, isocon analysis shows that 36 g of the original 75 g SiO_2 was removed from the protolith; only 0.6 g Na_2O had to be added to the 7.7 g Na_2O already present there. This gain in Na_2O is smaller than the gain in Fe_2O_{3Tot}, MgO, and CaO (2.2, 1.4, and 1.9 g, respectively) (see Appendix EA2 for detailed calculation). Note that because of the significant loss of SiO_2, Al_2O_3 was *passively* enriched (12.4 wt.% in protolith vs. 18.1 wt.% in jadeitite), despite being completely immobile during the process. The slight mismatch in the contents of oxides, including Fe_2O_{3Tot}, MgO, CaO, and Na_2O, can be explained either by a "true" mass gain from the metasomatizing fluid or by a not completely representative sampling of the rim and core of the tectonic block. These calculations strongly support the R-type nature of the Monviso jadeitite, as originally proposed by Compagnoni et al. (2012), and demonstrate that simple desilication of an oceanic plagiogranite (or its isochemical metamorphic equivalent) can be responsible for the formation of R-type jadeitites. The above analysis of the Monviso example shows that an "unrealistically complex" chemical exchange is not a prerequisite for the formation of an R-type jadeitite.

Mass transfer during metasomatic replacement of oceanic plagiogranite: application of isocon analysis to jadeite rocks of the RSJC

Isocon analysis will now be applied to jadeitites and related rocks from the RSJC to investigate a possible R-type origin. Although in contrast to the Monviso jadeitite there are no direct links between the RSJC jadeite rocks and their potential protoliths, the following systematic approach offers some useful estimates for the necessary mass transfer to be expected during metasomatism. Since several samples of the matrix-quartz-bearing suite had already been identified as representing isochemical metamorphic equivalents of oceanic plagiogranites (see section 6.1), the composition of the concordant jadeite–lawsonite quartzite (sample 30772) was taken to be that of a potential protolith. Furthermore, the chemical compositions of oceanic plagiogranites from Newfoundland (suprasubduction-zone ophiolite, SSZ-O (Malpas, 1979)), the Mid-Atlantic Ridge (MOR (Aumento, 1969)), and Chile (SSZ-O (Saunders et al., 1979)) from the compilation of Koepke et al. (2004) were used as those of potential protoliths. Among these four protoliths, sample 30772 is the most SiO_2-rich (72 wt.%), whereas the oceanic plagiogranite from Newfoundland possesses the lowest SiO_2 (60 wt.%) in combination with the highest Na_2O (8 wt.%) contents; the oceanic plagiogranite from the Mid-Atlantic Ridge possesses intermediate SiO_2 (62 wt.%) and Na_2O (6 wt.%) contents, and the one from Chile shows the lowest Na_2O (2 wt.%) contents. These four hypothetical protoliths represent a useful range of Fe_2O_3, MgO, and CaO contents (Table 6). Next, isocon analysis will be performed on eight jadeite rocks from the present study. Six of them are from the chemical group I (Na_2O-rich; samples 30023, 30046, 30065, 30852, 31034, and 31049, see Fig. 12*a*), and two belong to group II (Na_2O-poor; samples 30824 and 30853). Only sample 30046, the concordant jadeitite, is from the matrix-quartz-bearing suite.

Figure 14 shows the calculated gains and losses of the oxides SiO_2, Fe_2O_{3Tot}, CaO, MgO, and Na_2O in g per 100 g protolith associated with the assumed metasomatic replacement of the four protolith compositions by their respective jadeite rocks (see Appendix EA3 for detailed values). For example, to alter a protolith with the composition of sample 30772 so as to attain the chemical composition of sample 30046 (Fig. 14*a*), SiO_2 (absolute loss or gain, mass in protolith; –22.3 g and 71.8 g), Fe_2O_{3Tot} (–0.6 g and 1.2 g), and CaO (–2.3 g and 3.3 g) have to be removed from the protolith (100 g), whereas MgO (+0.3 g and 0.5 g) and Na_2O (+2.8 g and 5.6 g) have to be added to the protolith. For this protolith composition, the calculated loss of SiO_2 may reach –41.3 g (sample 30824). The necessary gain in Na_2O ranges from +1.4 (sample 31049) to +3.5 g (sample 30852); replacement by samples 30824 and 30853 necessitates Na_2O loss (–0.9 g and –0.8 g, respectively). Note that both these and the following comparisons assume Al_2O_3 to be completely immobile. Despite being considerably less SiO_2-rich and more Na_2O-rich than sample 30772 (Table 6), the Newfoundland plagiogranite (Fig. 14*b*) would require similar amounts of Na_2O loss or gain (+2.3 g to +3.3 g and ~–2.3 g). SiO_2 would need to be added (+2.5 g) to replace the Newfoundland plagiogranite by the concordant jadeitite. In the case of the plagiogranites from the Mid-Atlantic Ridge (Fig. 14*c*) and Chile (Fig. 14*d*), successively higher amounts of Na_2O would need to be gained by the protolith during metasomatism (up to +4.7 g and up to +6.8 g, respectively).

The simplest conceivable metasomatic process that would transform a felsic protolith into an SiO_2-undersaturated rock, such as a jadeitite, necessarily involves desilication of the precursor; hence, pure desilication is treated here as the optimal, i.e., least complex process. This means that only small amounts of the other oxides are allowed to be gained or lost during metasomatism. To judge whether the calculated mass gains or losses satisfy this condition, it is helpful to examine once again the results from the Monviso jadeitite (Compagnoni et al., 2012), since it represents the best-case scenario in this context. For the formation of this widely recognized R-type jadeitite, +2.2, +1.4, and +1.9 g Fe_2O_{3Tot}, MgO, and CaO, respectively, had to be nominally "added" to the protolith (see Appendix EA2). Therefore, we consider mass gains or losses in these oxides in the range of ~±3 g per 100 g protolith as acceptable and realistic. Only a minor amount of Na_2O (+0.6 g) was gained during metasomatism, making it more difficult to define an upper limit for the accepted amount of Na_2O increase. Based on these considerations and results of the isocon analysis, we conclude that sample 30772 is an appropriate protolith for samples 31049 and 30824; the Newfoundland plagiogranite pairs well with sample 31049; the Mid-Atlantic Ridge plagiogranite, with samples 30824 and 30853. Therefore, jadeite rocks of the chemical group II (samples 30824 and 30853), as well as the least Na_2O-rich jadeitite (sample 31049), can be readily obtained by metasomatic replacement of plausible oceanic plagiogranites by straightforward desilication, a process that seems realistic in a serpentinite-rich environment. If changes in Na_2O of up to ~±3 g per 100 g protolith are allowed, sample 30772, as well as the Newfoundland plagiogranite, could serve as suitable precursor rocks for most of the jadeitites and jadeite rocks considered in this study.

The problem of missing relict textures in jadeitites—zircon as a potential igneous relict mineral

No relics of igneous plagioclase or pyroxene have been observed in jadeite rocks from the RSJC so far. With the exception of the Monviso jadeitite, the lack of igneous relict textures and minerals is a general feature

of jadeitites and poses a serious problem for models that invoke metasomatism as the dominant mode of formation (Harlow et al., 2014). Zircon, a common accessory mineral in jadeitites, can withstand high-grade metamorphism or anatexis and be of igneous, hydrothermal, and metamorphic origin (Valley, 2003; Harley and Kelly, 2007; Page et al., 2007; Rubatto and Hermann, 2007; Fu et al., 2012). Due to its high resistance in high-*T* and -*P* environments, zircon represents a potential relict mineral that can be inherited from precursor rocks, such as oceanic plagiogranites. However, zircon in jadeitites might also have crystallized coevally with the jadeite from a fluid (or hydrous melt) or represent (igneous) xenocrysts assimilated from a wall rock or carried by the fluid to the location of jadeitite genesis. A number of studies have demonstrated that it is possible to distinguish igneous from hydrothermal (and metamorphic) zircon by analyzing their REE and trace-element (Schaltegger et al., 1999; Rubatto, 2002; Hoskin and Schaltegger, 2003; Hoskin, 2005; Geisler et al., 2007; Rubatto and Hermann, 2007; Mattinson et al., 2009; McClelland et al., 2009) as well as oxygen isotope compositions (Valley et al., 2003; Page et al., 2007). Furthermore, abundant fluid inclusions ($H_2O + CH_4$) suggest a hydrothermal origin for the respective zircon domains (Tsujimori, 2017). However, the classification of zircon as either igneous or hydrothermal must be performed on a case-by-case basis, since there are no universally valid methods available for discriminating between them (Harley and Kelly, 2007).

The problems involved in unequivocally differentiating igneous from hydrothermal zircon have led to different interpretations regarding the origin of zircon in jadeitites. For example, a hydrothermal origin was proposed in Tsujimori et al. (2005); Bröcker and Keasling (2006); Qiu et al. (2009); Cárdenas-Párraga et al. (2012); Schertl et al. (2012); Flores et al. (2013), whereas an igneous origin for at least a fraction of the analyzed zircon was advocated in Shi et al. (2008); Fu et al. (2010, 2012); Mori et al. (2011); Yui et al. (2012, 2013); Hertwig et al. (2016); Meng et al. (2016). The presence of exclusively hydrothermal zircon populations has generally been taken as strong evidence for a P-type origin of the respective jadeitites, whereas igneous zircon cores in zoned crystals have been interpreted in different ways: either as xenocrysts originating from reworked subducted crust and deposited by the jadeitite-forming fluid (e.g., the Syum-Keu complex, Polar Urals (Meng et al., 2016)) or as relict crystals inherited directly from a recrystallized igneous protolith (RSJC) (Hertwig, 2014; Hertwig et al., 2016).

Zircon has also been studied in detail from a suite of samples from the RSJC jadeite rocks (Hertwig, 2014; Hertwig et al., 2016). Zircon was separated from two albite-bearing jadeite rocks (samples 30790b and 30824) as well as from the concordant jadeitite (sample 30046) and its jadeite–blueschist country rock (sample 30045). All of these rocks contain igneous zircon of similar age (ca. 117–113 Ma), interpreted to be inherited from magmatic protoliths. In the case of zircon from the concordant jadeitite, younger (ca. 78 Ma) zircon domains of hydrothermal origin were identified, and their origin was tentatively linked to the jadeitite-forming event (Hertwig et al., 2016). Furthermore, in an earlier study on zircon from an individual jadeitite from the RSJC (sample 30071 in Schertl et al. (2012)), zircon cores with ages of ~115 Ma were found and originally interpreted to be of hydrothermal origin; however, REE patterns and trace-element characteristics obtained subsequently also lend credence to an igneous origin of this zircon. In summary, four different jadeite rocks from various sampling locations within the RSJC possess igneous zircon of roughly similar age. While it cannot be ruled out that all of the zircon grains from all four jadeite rocks were deposited by the jadeite-forming fluid, this conclusion seems fortuitous, and the most straightforward explanation for the RSJC is clearly that zircon was inherited from a precursor igneous protolith. To clarify discussions on the significance of igneous zircon in other occurrences, we suggest that additional accessory minerals commonly found in jadeitites and other mélange rocks, such as rutile, titanite, monazite, and apatite, should be studied. For instance, in situ U–Pb age dating of titanite and rutile could provide additional constraints on the timing of jadeitite formation or, alternatively, on the timing of magmatic growth. Comparison with zircon ages would provide information on their origin and help to decide whether zircon truly represents one of the rare igneous relict phases in jadeitites.

In addition, the impact and potential significance of mineral-inclusion studies in zircon and other accessory minerals, such as titanite and rutile, which can represent rigid time capsules preserving early rock histories, has been documented by Schertl and Schreyer (1996), Liu and Liou (2011) and Schertl et al. (2019). Nevertheless, careful scrutiny of zircon domains with methods, such as cathodoluminescence microscopy, is important to correctly relate potential magmatic or metamorphic mineral inclusions to the respective host zircon ages and to distinguish so-called *pseudoinclusions* from primary inclusions. For instance, during jadeitite formation, omphacite and jadeite can crystallize in small fissures and voids within (inherited) igneous zircon. If mistaken for primary inclusions, these pseudoinclusions can lead to the erroneous interpretation that zircon had crystallized at the same time as jadeite during the jadeitite-forming event (Schertl et al., 2019).

The problem of missing relict textures in jadeitites–quartz inclusions in jadeite crystals

In jadeite rocks from the RSJC, quartz inclusions were identified by electron microscopy in the matrix-quartz-free samples 30065 (jadeitite, Figs. 4*a–e*, 5*a*, 7*b*), 30769 (albite-rich phengite–jadeite rock, Fig. 3*g*), and

30790b (albite–jadeite rock, Figs. 3*h*, 4*f*). Furthermore, quartz inclusions in jadeite were discovered by Raman spectroscopy in samples 26322 (*jadeitite s.str.*) and 31034 (*jadeitite s.str.,* Fig. 3*e*) as an unexpected outcome of the comprehensive fluid inclusion study by Kawamoto et al. (2018). Owing to their very small size (~5 μm), such quartz inclusions are easily overlooked in conventional studies, suggesting further yet-to-be-identified cases among the RSJC samples. Quartz inclusions have also been found in the cores of jadeite grains from, for instance, the Mie and Tone jadeitites (Japan) and were interpreted by the authors to represent products of the breakdown of albite during prograde jadeitite genesis (Shigeno et al., 2005, 2012). Note that Zhang et al. (2014) have recently studied the prograde development of jadeite from albite starting material experimentally. Their experiments yielded very similarly textured jadeite grains with cloudy cores containing minute quartz inclusions. Therefore, these quartz inclusions in the RSJC samples may well represent indirect evidence for former, now-replaced igneous plagioclase and the existence of a precursor rock. Nevertheless, Harlow et al. (2014) also argue that such jadeite crystals might have formed from silica-saturated fluids or that jadeitite-forming fluids "enveloped and invaded" (Harlow et al., 2014) overprinted plagiogranites in which igneous plagioclase had already reacted to jadeite and quartz. In the latter case, the distinction between R- and P-type jadeitite might be merely a matter of the dimensions of a sample and from where within a tectonic block it was taken.

Most jadeitites are albite-bearing and silica-undersaturated rocks (Harlow et al., 2014). If jadeite and albite formed at equilibrium conditions from an aqueous fluid, jadeite should crystallize without quartz inclusions. The presence of such inclusions in jadeite of a sizable fraction of the matrix-quartz-free and albite-bearing rocks of the RSJC suggests that in these rocks the jadeite grains did not crystallize in equilibrium with the surrounding albite. The anhedral grain shapes of jadeite in samples 30065 (Fig. 5*a*), 30769 (Fig. 3*g*), and 26322 support this conclusion; however, this criterion is not entirely reliable. Even though jadeite is euhedral in sample 31034, quartz inclusions were still identified by Raman spectroscopy (Kawamoto et al., 2018). In sample 30065, anhedral and unzoned jadeite shows overgrowths of omphacite, which indicates that omphacite rather than jadeite formed in equilibrium with the albite in the rock matrix.

In summary, we follow the interpretations of Shigeno et al. (2005, 2012) and suggest that in samples with predominantly anhedral jadeite and with quartz inclusions, the jadeite replaced a presumably igneous plagioclase at some stage of the rock formation history. This replacement would have occurred during an initial isochemical overprint of the igneous precursor rock (e.g., oceanic plagiogranite) at silica-saturated conditions. At this stage a jadeite–(lawsonite) quartzite would have formed. Later desilication and metasomatic overprinting would then have led to the final product, be it a jadeitite or another type of albite- and jadeite-rich rock. The suite of jadeite rocks in the RSJC may therefore document various stages in the transformation of oceanic plagiogranite into jadeitite. Hence, researchers should also be looking for relics of lawsonite and previous generations of jadeite and not only for igneous plagioclase and pyroxene to distinguish R- from P-type jadeitites.

The presence of fluids during jadeitite genesis: mixed P- and R-character

Jadeite crystals often exhibit rhythmical or oscillatory zoning patterns and contain fluid inclusions, attesting to the presence of a fluid phase during jadeitite genesis (Harlow, 1994; Sorensen et al., 2006; Harlow et al., 2011; Schertl et al., 2012; Takahashi et al., 2017; Kawamoto et al., 2018). Both features are also observed in jadeite from rocks of the RSJC (Fig. 3*f* [this study]; Schertl et al., 2012; Hertwig, 2014; Kawamoto et al., 2018) and demonstrate fluid-assisted jadeite crystallization, i.e., the defining feature of P-type genesis. It is of note, however, that in some samples (e.g., 26322, 30065, 30108, and 30769) either jadeite completely lacks oscillatory zonation patterns, or oscillatory zoning is limited to the rims and outer parts of the jadeite crystals. For instance, in sample 30023, cloudy, inclusion-rich cores are devoid of rhythmical zonation, while oscillatory zoning is well-developed in jadeite near the rim and close to the albite-filled interstitial voids (Fig. 5*b* in Schertl et al. (2012)). Therefore, we emphasize here that while there is considerable evidence for at least some degree of P-type formation in many jadeitites from the RSJC, fluid-assisted jadeite crystallization might not always be the dominant process. For a number of samples, desilication of plagiogranite (or its intermediate isochemical metamorphic equivalent) followed by late-stage fluid infiltration and precipitation of albite and jadeitic clinopyroxene would more accurately describe their mode of formation.

Kawamoto et al. (2018) studied fluid inclusions in a suite of six samples of the RSJC jadeite rocks, which included unequivocal P-type jadeite rock (discordant veins) as well as samples considered R-type on the basis of the criteria outlined in (Hertwig, 2014; Hertwig et al., 2016) and in this paper. Kawamoto et al. (2018) found that the aqueous fluid composition (slightly more saline than seawater) and entrapment conditions were essentially the same in all the inclusions studied. Kawamoto et al. (2018) concluded that there must be a strong genetic link between P- and R-type genesis in the RSJC. In their most recent review, Harlow et al. (2014, p. 26) now also express the opinion that different blocks from the same jadeitite occurrence can show different degrees of P- and R-type formation.

Little attention appears to have been given to the actual physical process of potentially opening and maintaining voids at high pressure in serpentinized ultramafic rocks for the precipitation of P-type jadeitite. The only unequivocal P-type jadeite-rich rocks in our study are the discordant veins of matrix-quartz-bearing rock types in blueschist blocks. However, these veins are very inhomogeneous. Thin-section and cathodoluminescence studies show that they are aggregates of several generations of crack-seal events (Schertl et al., 2012). Jadeite and lawsonite crystals grow as palisade arrays or radial sprays from hairline fractures in a quartz matrix (Figs. 3*c* and 5*g* in Schertl et al. (2012)). Our study thus cannot help to clarify the question of primary P-type precipitation in serpentinite.

As noted above, our repeated observation of cloudy, inclusion-rich cores of jadeite grains devoid of rhythmical zonation with rims of jadeite with well-developed oscillatory zoning, especially near albite-filled interstitial voids, leads us to propose the following scenario. Note that isochemical recrystallization of a plagiogranite to a jadeite-rich rock must lead to a reduction in volume due to the increase in rock density. As a rough preliminary estimate, we can assume a considerable (about 10%) decrease in volume at 15 kbar. These voids provide pathways for the saline fluids present in the surrounding serpentinite. The interface between plagiogranite dikes and their surroundings (tectonic blocks or serpentinite) would also be an appropriate "persistent" fluid pathway, as suggested recently by Angiboust et al. (2020). Euhedral jadeite with oscillatory zoning can grow in these fluid-filled voids, as we observed in our samples. Little is known about silicate solubility in saline fluids at ≈350 °C/17 kbar. However, extrapolating the solubility data of Wohlers et al. (2011) in the simple system Na–Al–Si in pure water down to these *PT*-conditions would indicate that the solute will be dominated, as might be expected, by Si, followed by Na and Al. Thus, while the observed desilication appears realistic, non-negligible amounts of jadeite component can also be mobilized. Circulating fluids can act both as a metasomatic agent and as a vehicle of redistribution, as in the observed discordant veins. As discussed in Kawamoto et al. (2018), there is good evidence for the fact that serpentinization was still active in the RSJC mélanges during jadeitite formation, so that the surrounding ultramafic envelope constituted an active sink for Si. At the same time, the mélanges contain many blackwall blocks rich in actinolite, and chlorite indicating Si transfer was active irrespective of the degree of serpentinization of the ultramafic host.

CONCLUSIONS

The major result of this study is the verification that many of the jadeite-rich rocks in the serpentinite mélanges of the Río San Juan Complex in the northern Dominican Republic might have developed from an igneous protolith. The process was very likely fluid-enhanced, but the main mass of these rocks did not crystallize directly from an aqueous fluid. In these rocks, oscillatory zoning in jadeite reflecting open-system crystallization, when observed, is restricted to crystal rims and overgrowths. This study corroborates the conclusions of Hertwig (2014) and Hertwig et al. (2016) based on the study of zircon.

The rich diversity of jadeite-bearing rocks available in the RSJC allows important trends to be distinguished. These trends in whole-rock chemistry can be correlated with a logical genetic succession leading from oceanic plagiogranite protolith to rocks of the matrix-quartz-bearing suite and finally to those of the matrix-quartz-free suite. The first step, from plagiogranite protolith to the quartz-rich varieties of the matrix-quartz-bearing suite, is an isochemical high-pressure overprint. The relative proportions of jadeite and lawsonite in this suite depend on the specific plagioclase composition of the protolith. The second step involves predominant desilication, mirroring the silica-undersaturated environment of the serpentinite matrix of the mélange. The presence of remnant quartz inclusions in jadeite inherited from plagioclase breakdown suggests that this reaction path was taken. This array of samples mirrors the reaction path in a single block described by Compagnoni et al. (2012), where the jadeite–quartz core of the block grades outward toward the serpentinite host into a *jadeitite s.str*. Alternatively, the high-pressure overprint and desilication might be coeval, and the plagiogranite might have developed directly into a rock of the matrix-quartz-free suite. Quartz inclusions in jadeite would then be rare or absent.

As the array of samples observed in the RSJC appears to reflect a reaction sequence, each individual sample may represent a different stage in development. Each sample must be studied individually to define its reaction history. Studies on zircon have provided valuable new data, but open questions remain. Future studies should therefore emphasize the role of additional accessory minerals, such as rutile, monazite, titanite, and apatite. Detailed studies on these accessories have the potential to greatly enhance our understanding of jadeitite genesis.

We thank T. Tsujimori and an anonymous reviewer for helpful comments. We are grateful to T. Murad for help with sample handling, H.-J. Bernhardt for assistance with EPMA analysis, and T. Fockenberg for performing whole-rock geochemical analysis. This work was supported by DFG grant SCHE 517/10-1 to HPS and WVM

REFERENCES

Aldiss, D.T., 1981. Plagiogranites from the ocean crust and ophiolites. Nature 289, 577–578, doi: 10.1038/289577a0.

Angiboust, S., Glodny, J., Cambeses, A., Raimondo, T., Monié, P., Popov, M., Garcia-Casco, A., 2020. Drainage of subduction interface fluids into the forearc mantle evidenced by a pristine jadeitite network (Polar Urals). J. Metamorph. Geol., doi: 10.1111/jmg.12570.

Aumento, F., 1969. Diorites from the Mid-Atlantic Ridge at 45°N. Science 165 (3898), 1112–1113, doi: 10.1126/science.165.3898.1112.

Bernhardt, H.-J., 2010. MINCALC-V5 a non EXCEL based computer program for general electron-microprobe mineral analyses data processing, in: Abstract of 20th IMA-Meeting, session XO150G, 869.

Boschman, L.M., van Hinsbergen, D.J.J., Torsvik, T.H., Spakman, W., Pindell, J.L., 2014. Kinematic reconstruction of the Caribbean region since the Early Jurassic. Earth Sci. Rev. 138, 102–136, doi: 10.1016/j.earscirev.2014.08.007.

Bröcker, M., Keasling, A., 2006. Ionprobe U-Pb zircon ages from the high-pressure/low-temperature mélange of Syros, Greece: Age diversity and the importance of pre-Eocene subduction. J. Metamorph. Geol. 24 (7), 615–631, doi: 10.1111/j.1525-1314.2006.00658.x.

Cárdenas-Párraga, J., García-Casco, A., Harlow, G.E., Blanco-Quintero, I.F., Rojas-Agramonte, Y., Kröner, A., 2012. Hydrothermal origin and age of jadeitites from Sierra del Convento Mélange. Eur. J. Mineral. 24 (2), 313–331, doi: 10.1127/0935-1221/2012/0024-2171.

Coleman, R.G., 1961. Jadeite deposits of the Clear Creek Area, New Idria District, San Benito Country, California. J. Petrol. 2, 209–247, doi: 10.1093/petrology/2.2.209.

Coleman, R.G., 1977. Ophiolites. Springer, Berlin, doi: 10.1007/978-3-642-66673-5.

Coleman, R.G., Donato, M.M., 1979. Oceanic plagiogranite revisited, in: Barker, F. (Ed.), Trondhjemites, Dacites, and Related Rocks. Elsevier, Amsterdam, pp. 149–167.

Compagnoni, R., Rolfo, F., Castelli, D., 2012. Jadeitite from the Monviso meta-ophiolite, western Alps: occurrence and genesis. Eur. J. Mineral. 24, 333–343, doi: 10.1127/0935-1221/2011/0023-2164.

Dobretsov, N.L., Ponomareva, L.G., 1965. Comparative characteristics of jadeite and associated rocks from Polar Ural and Prebalkhash region. Int. Geol. Rev. 10 (2), 221—242.

Escuder-Viruete, J., 2010. Mapa Geológico de la República Dominica. Escala 1:50,000. Hojas de Río San Juan, Guayabito, Salcedo, Gaspar Hernández, Pimentel, Cabrera y Villa Riva. Instituto Geológico y Minero de España, Santo Domingo, R.D.

Escuder-Viruete, J., Valverde-Vaquero, P., Rojas-Agramonte, Y., Jabites, J., Pérez-Estaún, A., 2013. From intra-oceanic subduction to arc accretion and arc-continent collision: Insights from the structural evolution of the Río San Juan metamorphic complex, northern Hispaniola. J. Struct. Geol. 46, 34–56, doi: 10.1016/j.jsg.2012.10.008.

Evans, B.E., 1977. Metamorphism of Alpine peridotite and serpentinite. Annu. Rev. Earth Planet. Sci. 5, 397–447, doi: 10.1146/annurev.ea.05.050177.002145 .

Flores, K.E., Martens, U.C., Harlow, G.E., Brueckner, H.K., Pearson, N.J., 2013. Jadeitite formed during subduction: In situ zircon geochronology constraints from two different tectonic events within the Guatemala Suture Zone. Earth Planet. Sci. Lett. 371–372, 67–81, doi: 10.1016/j.epsl.2013.04.015.

Flores, K.E., Hemming, S.R., Harlow, G.E., Cai, Y., Bonnet, G., Martin, C., Brueckner, H.K., 2014. Metamorphic evolution of high-pressure-low-temperature rocks from the northern section of the Guatemala Suture Zone: PTt paths and tectonic implications. AGU Fall Meeting, V43B-4883.

Fu, B., Valley, J.W., Kita, N.T., Spicuzza, M.J., Paton, C., Tsujimori, T., Bröcker, M., Harlow, G.E., 2010. Multiple origins of zircons in jadeitite. Contrib. Mineral. Petrol. 159, 769–780, doi: 10.1007/s00410-009-0453-y.

Fu, B., Paul, B., Cliff, J., Bröcker, M., Bulle, F., 2012. O–Hf isotope constraints on the origin of zircon in high-pressure mélange blocks and associated matrix rocks from Tinos and Syros, Greece. Eur. J. Mineral. 24, 277–287, doi: 10.1127/0935-1221/2011/0023-2131.

García-Casco, A., Rodriguez-Vega, A., Cárdenas-Párraga, J., Iturralde-Vinent, M.A., Lázaro, C., Blanco Quintero, I., Rojas-Agramonte, Y., Kröner, A., Núñez Cambra, K., Millan, G., Torres-Roldán, R.L., Carrasquilla, S., 2009. A new jadeitite jade locality (Sierra del Convento, Cuba): first report and some petrological and archeological implications. Contrib. Mineral. Petrol. 158, 1, doi: 10.1007/s00410-008-0367-0.

García-Casco, A., Knippenberg, S., Ramos, R.R., Harlow, G.E., Hofman, C., Pomo, J.C., Blanco Quintero, I., 2013. Pre-Columbian jadeitite artifacts from the Golden 1 Rock Site, St. Eustatius, Lesser Antilles, with special reference to jadeitite artifacts from Elliot's, Antigua: Implications for potential source regions

and long-distance exchange networks in the Greater Caribbean. J. Archaeol. Sci. 40, 3153–3169, doi: 10.1016/j.jas.2013.03.025.

Geisler, T., Schaltegger, U., Tomaschek, F., 2007. Re-equilibration of zircon in aqueous fluids and melts. Elements 3, 43–50, doi: 10.2113/gselements.3.1.43.

Gerya, T.V., Stöckhert, B., Perchuk, A.L., 2002. Exhumation of high-pressure metamorphic rocks in a subduction channel: A numerical simulation. Tectonics 21 (6), 6-1—6-19, doi: 10.1029/2002TC001406.

Grant, J.A., 1986. The isocon diagram; a simple solution to Gresens' equation for metasomatic alteration. Econ. Geol. 81 (8), 1976–1982, doi: 10.1016/j.pce.2004.11.003.

Grant, J.A., 2005. Isocon analysis: A brief review of the method and applications. Phys. Chem. Earth Parts A–C 30, 997–1004, doi: 10.1016/j.pce.2004.11.003.

Harley, S.L., Kelly, N.M., 2007. Zircon: Tiny but timely. Elements 3 (1), 13–18, doi: 10.2113/gselements.3.1.25.

Harlow, G.E., 1994. Jadeitites, albitites and related rocks from the Motagua Fault Zone, Guatemala. J. Metamorph. Geol. 12 (1), 49–68, doi: 10.1111/j.1525-1314.1994.tb00003.x.

Harlow, G.E., Sorensen, S.S., 2005. Jade (nephrite and jadeitite) and serpentinite: metasomatic connections. Int. Geol. Rev. 47 (2), 113–146, doi: 10.2747/0020-6814.47.2.113.

Harlow, G.E., Murphy, A.R., Hozjan, D.J., de Mille, C.N., Levinson, A.A., 2006. Pre-Columbian jadeite axes from Antigua, West Indies: Description and possible sources. Can. Mineral. 44, 305–321, doi: 10.2113/gscanmin.44.2.305.

Harlow, G.E., Sorensen, S.S., Sisson, V.B., 2007. Jade, in: Groat, L.A. (Ed.), The Geology of Gem Deposits. Short Course Handbook Ser. 37, Mineral. Assoc. Canada Quebec, pp. 207–254.

Harlow, G.E., Sisson, V.B., Sorensen, S.S., 2011. Jadeitite from Guatemala: New observations and distinctions among multiple occurrences. Geol. Acta 9, 363–387.

Harlow, G.E., Sorensen, S.S., Sisson, V.B., Shi, G., 2014. The geology of jade deposits, in: Groat, L.A. (Ed.), The Geology of Gem Deposits, 2nd ed. Short Course Handbook Ser. 44, Mineral. Assoc. Canada, Quebec, pp. 305–374, doi: 10.1344/105.000001694.

Harlow, G.E., Berman, M.J., Cárdenas-Párraga, J., Hertwig, A., García-Casco, A., Gnivecki, P.L., 2019. Pre-Columbian jadeitite artifacts from San Salvador Island, Bahamas and comparison with jades of the eastern Caribbean and jadeitites of the greater Caribbean region. J. Archaeol. Sci., Rep. 26, 101830.

Hawthorne, F.C., Oberti, R., Harlow, G.E., Maresch, W.V., Martin, R.F., Schumacher, J.C., Welch, M.D., 2012. Nomenclature of the amphibole supergroup. Am. Mineral. 97, 2031–2048, doi: 10.2138/am.2012.4276.

Hertwig, A., 2014. Genesis of jadeitites and their country rocks, Rio San Juan Complex, Dominican Republic. PhD Dissertation, Ruhr-University. Bochum, Bochum.

Hertwig, A., McClelland, W.C., Kitajima, K., Schertl, H.-P., Maresch, W.V., Stanek, K., Valley, J.W., Sergeev, S.A., 2016. Inherited igneous zircons in jadeitite predate high-pressure metamorphism and jadeitite formation in the Jagua Clara serpentinite mélange of the Rio San Juan Complex (Dominican Republic). Contrib. Mineral. Petrol. 171, 48, doi: 10.1007/s00410-016-1256-6.

Hofman, C.L., Bright, A.J., Boomert, A., Knippenberg, S., 2007. Island rhythms: The web of social relationships and interaction networks in the Lesser Antillean Archipelago between 400 B.C. and A.D. 1492. Lat. Am. Antiq. 18 (3), 243–268, doi: 10.2307/25478180.

Hofman, C.L., Boomert, A.J., Bright, A.J., Rodríguez Ramos, R., 2010. Crossing the Caribbean Sea: towards a holistic view of pre-colonial mobility and exchange. J. Caribb. Archaeol., Spec. Publ. 3.

Hofman, C.L., Boomert, A., Bright, A.J., Hoogland, M.L.P., Knippenberg, S., Sampson, A.V.M., 2011. Ties with the homelands: archipelagic interaction and the enduring role of the South American mainlands in the Pre-Columbian Lesser Antilles, in: Curet, L.A., Hauser, M.W. (Eds.), Islands at the Crossroads, Migration, Seafaring, and Interaction in the Caribbean. University of Alabama Press, Tuscaloosa, Alabama.

Hofman, C., Mol, A., Hoogland, M., Valcárcel Rojas, R., 2014. Stage of encounters: migration, mobility and interaction in the pre-colonial and early colonial Caribbean. World Archaeol. 46, 590–609, doi: 10.1080/00438243.2014.925820.

Hoskin, P.W.O., 2005. Trace-element composition of hydrothermal zircon and the alteration of Hadean zircon from the Jack Hills, Australia. Geochim. Cosmochim. Acta 69, 637–648, doi: 10.1016/j.gca.2004.07.006.

Hoskin, W.O., Schaltegger, U., 2003. The composition of zircon and igneous and metamorphic petrogenesis, in: Hanchar, J.M., Hoskin, W.O. (Eds.), Zircon. Mineral. Soc. Am., Geochem. Soc., Washington, D.C., pp. 27–55.

Iturralde-Vinent, M.A., 1994. Tectonostratigraphic correlation of the NW Caribbean: Dominican Republic. J. Pet. Geol. 17, 243–245.

Kawamoto, T., Hertwig, A., Schertl, H.-P., Maresch, W.V., 2018. Fluid inclusions in jadeitite and jadeite-rich rock from serpentinite mélanges in northern Hispaniola: Trapped ambient fluids in a cold subduction channel. Lithos 308–309, 227–241, doi: 10.1016/j.lithos.2018.02.024.

Keverne, R., 2010. Jade. Aquamarine, London.

Knippenberg, S., 2007. Stone Artifact Production and Exchange among the Lesser Antilles. ASLU, Leiden Univ. Press, Leiden.

Knippenberg, S., 2011. Much to choose from. The use and distribution of siliceous stone in the Lesser Antilles, in: Hofman, C., van Duijvenbode, A. (Eds.), Communities in Contact. Essays in Archaeology, Ethnohistory and Ethnography of the Amerindian Circum-Caribbean. Sidestone Press, Leiden, pp. 171–186.

Koepke, J., Feig, S.T., Snow, J., Freise, M., 2004. Petrogenesis of oceanic plagiogranites by partial melting of gabbros: an experimental study. Contrib. Mineral. Petrol. 146, 414–432, doi: 10.1007/s00410-003-0511-9.

Koepke, J., Berndt, J., Feig, S.T., Holtz, F., 2007. The formation of SiO2-rich melts within the deep oceanic crust by hydrous partial melting of gabbros. Contrib. Mineral. Petrol. 153, 67–84,doi: 10.1007/s00410-006-0135-y.

Krebs, M., 2008. Druck-Temperatur-Zeit-Pfade subduktionszonenbezogener Hochdruckmetamorphite des Rio San Juan-Komplexes, Dominikanische Republik. PhD Dissertation, Ruhr-Univ. Bochum.

Krebs, M., Schertl, H.-P., Maresch, W.V., Draper, G., 2011. Mass flow in serpentinite-hosted subduction channels: P-T-t path patterns of metamorphic blocks in the Rio San Juan mélange (Dominican Republic). J. Asian Earth Sci. 42, 569–595, doi: 10.1016/j.jseaes.2011.01.011.

Leake, B.E., Woolley, A.R., Arps, C.E.A., Birch, W.D., Gilbert, M.C., Grice, J.D., Hawthorne, F.C., Kato, A., Kisch, H.J., Krivovichev, V.G., Linthout, K., Laird, J., Mandarino, J.M., Maresch, W.V., Nickel, E.H., Rock, N.M.S, Schumacher, J.C., Smith, D.C., Stephenson, N.C.N., Ungaretti, L., Whittaker, E.J.W., Youzhi, G., 1997. Nomenclature of amphiboles; report of the subcommittee on amphiboles of the International Mineralogical Association, Commission on New Minerals and Mineral Names. Can. Mineral. 35, 219–246.

Le Maitre, R.W., 2002. Igneous Rocks. Cambridge Univ. Press, Cambridge.

Liu, F.L., Liou, J.G., 2011. Zircon as the best mineral for *P–T–*time history of UHP metamorphism: A review on mineral inclusions and U–Pb SHRIMP ages of zircons from the Dabie–Sulu UHP rocks. J. Asian Earth Sci. 40, 1–39, doi: 10.1016/j.jseaes.2010.08.007.

Malpas, J., 1979. Two contrasting trondhjemite associations from transported ophiolites in Western Newfoundland: Initial report, in: Barker, F. (Ed.), Trondhjemites, Dacites, and Related Rocks. Elsevier, Amsterdam, pp. 465–487.

Maresch, W.V., Grevel, C., Stanek, K.P., Schertl, H.-P., Carpenter, M.A., 2012. Multiple growth mechanisms of jadeite in Cuban metabasite. Eur. J. Mineral. 24, 217–235, doi: 10.1127/0935-1221/2012/0024-2179.

Mattinson, C.G., Wooden, J.L., Zhang, J.X., Bird, D.K., 2009. Paragneiss zircon geochronology and trace element geochemistry, North Qaidam HP/UHP terrane, western China. J. Asian Earth Sci. 35, 298–309, doi: 10.1016/j.jseaes.2008.12.007.

McClelland, W.C., Gilotti, J.A., Mazdab, F.K., Wooden, J.L., 2009. Trace-element record in zircons during exhumation from UHP conditions, North-East Greenland Caledonides. Eur. J. Mineral. 21, 1135–1148, doi: 10.1127/0935-1221/2009/0021-2000.

Meng, F., Yang, H.-J., Makeyev, A.B., Ren, Y., Kulikova, K.V., Bryanchaninova, N.I., 2016. Jadeitite in the Syum-Keu ultramafic complex from Polar Urals, Russia: insights into fluid activity in subduction zones. Eur. J. Mineral. 28, 1079–1097, doi: 10.1127/ejm/2016/0028-2563.

Millán, G., Somin, M., 1981. Litología, estratigrafía, tectónica y metamorfismo del macizo de Escambray. Editorial Academica, La Habana.

Millero, F.J., Feistel, R., Wright, D.G., McDougall, T.J., 2008. The composition of Standard Seawater and the definition of the Reference-Composition Salinity Scale. Deep Sea Res. Part I: Oceanogr. Res. Pap. 55, 50–72, doi: 10.1016/j.dsr.2007.10.001.

Mori, Y., Orihashi, Y., Miyamoto, T., Shimada, K., Shigeno, M., Nishiyama, T., 2011. Origin of zircon in jadeitite from the Nishisonogi metamorphic rocks, Kyushu, Japan. J. Metamorph. Geol. 29, 673–684, doi: 10.1111/j.1525-1314.2011.00935.x.

Morimoto, N., Fabries, J., Ferguson, A.K., Ginzburg, I.V., Ross, M., Seifert, F.A., Zussman, J., Aoki, K., Gottardi, G., 1988. Nomenclature of pyroxenes. Am. Mineral. 73, 1123–1133.

Niu, Y., Gilmore, T., Mackie, S., Greig, A., Bach, W., 2002. Mineral chemistry, whole-rock compositions, and petrogenesis of leg 176 gabbros: Data and discussion, in: Natland, J.H., Dick, H.J.B., Miller, D.J., von Herzen, R.P. (Eds.), Proceedings of the Ocean Drilling Program, Scientific Results, Vol. 176. Natl. Sci. Foundation, pp. 1–60, doi: 10.2973/odp.proc.sr.176.011.2002.

Page, F.Z., Ushikubo, T., Kita, N.T., Riciputi, L.R., Valley, J.W., 2007. High-precision oxygen isotope analysis of picogram samples reveals 2 μm gradients and slow diffusion in zircon. Am. Mineral. 92 (10), 1772–1775, doi: 10.2138/am.2007.2697.

Pindell, J.L., Kennan, L., 2009. Tectonic evolution of the Gulf of Mexico, Caribbean and northern South America in the mantle reference frame: an update, in: James, K.H., Lorente, M.A., Pindell, J.L. (Eds.), The Origin and Evolution of the Caribbean Plate. Geol. Soc. London Spec. Publ. 328, pp. 1–55, doi: 10.1144/SP328.1.

Pindell, J.L., Kennan, L., Maresch, W.V., Stanek, K.-P., Draper, G., Higgs, R., 2005. Plate-kinematics and crustal dynamics of circum-Caribbean arc-continent interactions: Tectonic controls on basin development in Proto-Caribbean margins, in: Caribbean-South American plate interactions, Venezuela. Geol. Soc. Am. Spec. Paper 394, pp. 7–52, doi: 10.1130/2005.2394(01).

Pindell, J.L., Maresch, W.V., Martens, U.C., Stanek, K.P., 2012. The Greater Antillean Arc: Early Cretaceous origin and proposed relationship to Central American subduction mélanges: implications for models of Caribbean evolution. Int. Geol. Rev. 54, 131–143, doi: 10.1080/00206814.2010.510008.

Qiu, Z., Wu, F., Yang, S., Zhu, M., Sun, J., Yang, P., 2009. Age and genesis of the Myanmar jadeite: Constraints from U-Pb ages and Hf isotopes of zircon inclusions. Chin. Sci. Bull. 54, 658–668, doi: 10.1007/s11434-008-0490-3.

Rieder, M., Cavazzini, G., D'yakonov, Y.S., Frank-Kamenetskii, V.A., Gottardi, G., Guggenheim, S., Koval', P.V., Müller, G., Neiva, A.M.R., Radoslovich, E.W., Robert, J.-L., Sassi, F.P., Takeda, H., Weiss, Z., Wones, D.R., 1998. Nomenclature of the micas. Can. Mineral. 36 (3), 905–912.

Rubatto, D., 2002. Zircon trace element geochemistry: partitioning with garnet and the link between U–Pb ages and metamorphism. Chem. Geol. 184, 123–138, doi: 10.1016/S0009-2541(01)00355-2.

Rubatto, D., Hermann, J., 2007. Zircon behaviour in deeply subducted rocks. Elements 3 (1), 31–35, doi: 10.2113/gselements.3.1.31.

Saunders, A.D., Tarney, J., Stern, C.R., Dalziel, I.W.D., 1979. Geochemistry of Mesozoic marginal basin floor igneous rocks from southern Chile. Geol. Soc. Am. Bull. 90 (3), 237–258, doi: 10.1130/0016-7606(1979)90<237:GOMMBF>2.0.CO;2.

Schaltegger, U., Fanning, C.M., Günther, D., Maurin, J.C., Schulmann, Gebauer, D., 1999. Growth, annealing and recrystallization of zircon and preservation of monazite in high-grade metamorphism: conventional and in-situ U-Pb isotope, cathodoluminescence and microchemical evidence. Contrib. Mineral. Petrol. 134, 186–201, doi: 10.1007/s004100050478.

Schertl, H.-P., Schreyer, W., 1996. Mineral inclusions in heavy minerals of the ultrahigh-pressure metamorphic rocks of the Dora Maira Massif and their bearing on the relative timing of the petrological events. Isotopic studies of crust-mantle evolution, in: Basu, A.R., Hart, S.R. (Eds.), Earth Processes: Reading the Isotopic Code. AGU, Geophys. Monograph 95, pp. 331–342, doi: 10.1029/GM095p0331.

Schertl, H.-P., Krebs, M., Maresch, W.V., Draper, G., 2007. Jadeitite from Hispaniola: a link between Guatemala and Antigua? in: 20th Colloquium on Latin American Earth Sciences, Kiel, Germany, Abstract Vol., pp. 167–168.

Schertl, H.-P., Maresch, W.V., Stanek, K.P., Hertwig, A., Krebs, M., Baese, R., Sergeev, S.S., 2012. New occurrences of jadeitite, jadeite quartzite and jadeite-lawsonite quartzite in the Dominican Republic, Hispaniola: petrological and geochronological overview. Eur. J. Mineral. 24, 199–216, doi: 10.1127/0935-1221/2012/0024-2201.

Schertl, H.-P., Maresch, W.V., Knippenberg, S., Hertwig, A., López Belando, A., Rodríguez Ramos, R., Speich, L., Hofman, C.L., 2018. Petrography, mineralogy and geochemistry of jadeite-rich artefacts from the Playa Grande excavation site, northern Hispaniola: evaluation of local provenance from the Río San Juan Complex. Geol. Soc. London Spec. Publ. SP474.3, pp. 231–253, doi: 10.1144/SP474.3.

Schertl, H.-P., Hertwig, A., Maresch, W.V., 2019. Cathodoluminescence microscopy of zircon in HP- and UHP-metamorphic rocks: A fundamental technique for assessing the problem of inclusions versus pseudo-inclusions. J. Earth Sci. 30, 1095–1107, doi: 10.1007/s12583-019-1246-5.

Schwartz, J.J., John, B.E., Cheadle, M.J., Wooden, J.L., Mazdab, F.K., Swapp, S., Grimes, C.B., 2010. Dissolution–reprecipitation of igneous zircon in mid-ocean ridge gabbro, Atlantis Bank, Southwest Indian Ridge. Chem. Geol. 274, 68–81, doi: 10.1016/j.chemgeo.2010.03.017.

Shi, G.-H., Cui, W., Cao, S., Jiang, N., Jian, P., Liu, D., Miao, L., Chu, B., 2008. Ion microprobe zircon U-Pb age and geochemistry of the Myanmar jadeitite. J. Geol. Soc. 165, 221–234, doi: 10.1144/0016-76492006-119.

Shigeno, M., Mori, Y., Nishiyama, T., 2005. Reaction microtextures in jadeitites from the Nishisonogi metamorphic rocks, Kyushu, Japan. J. Mineral. Petrol. Sci. 100, 237–246, doi: 10.2465/jmps.100.237.

Shigeno, M., Mori, Y., Shimada, K., Nishiyama, T., 2012. Jadeitites with metasomatic zoning from the Nishisonogi metamorphic rocks, western Japan: Fluid-tectonic block interaction during exhumation. Eur. J. Mineral. 24, 289–311, doi: 10.1127/0935-1221/2012/0024-2195.

Silva, Z.C.G., 1970. Origin of albitites from eastern Guatemala. Bol. Serv. Geol. Minas (Brazil) 22, 23–32.

Sorensen, S.S., Harlow, G.E., Rumble III, D., 2006. The origin of jadeitite-forming subduction-zone fluids: CL-guided SIMS oxygen-isotope and trace-element evidence. Am. Mineral. 91, 979–996, doi: 10.2138/am.2006.1949.

Stanek, K.P., Maresch, W.V., Scherer, E., Krebs, M., Berndt, J., Sergeev, S.S., Rodionov, N., Pfänder, J., Hames, W.E., 2019. Born in the Pacific and raised in the Caribbean: construction of the Escambray nappe stack, central Cuba. A review. Eur. J. Mineral. 31, 5–34, doi: 10.1127/ejm/2019/0031-2795.

Takahashi, N., Tsujimori, T., Kayama, M., Nishido, H., 2017. Cathodoluminescence petrography of P-type jadeitites from the New Idria serpentinite body, California. J. Mineral. Petrol. Sci. 112, 291–299, doi: 10.2465/jmps.170403.

Tsujimori, T., 2017. Early Paleozoic jadeitites in Japan: An overview. J. Mineral. Petrol. Sci. 112, 217–226, doi: 10.2465/jmps.170406a.

Tsujimori, T., Harlow, G.E., 2012. Petrogenetic relationships between jadeitite and associated high-pressure and low-temperature metamorphic rocks in worldwide jadeitite localities: a review. Eur. J. Mineral. 24, 371–390, doi: 10.1127/0935-1221/2012/0024-2193.

Tsujimori, T., Wooden, J., Miyamoto, T., 2005. U-Pb dating of large zircons in low-temperature jadeitite from the Osayama serpentinite melange, Southwest Japan: Insights into the timing of serpentinization. Int. Geol. Rev. 47, 1048–1057, doi: 10.2747/0020-6814.47.10.1048.

Ungethüm, H., 1965. Eine neue Methode zur Bestimmung von Eisen (II) in Gesteinen und Mineralen, insbesondere auch in bitumenhaltigen Proben. Z. Angew. Geol. 11 (9), 500–505.

Valley, J.W., 2003. Oxygen isotopes in zircon, in: Hanchar, J.M., Hoskin, W.O. (Eds.), Zircon. Mineral. Soc. Am., Geochem. Soc., Washington, D.C., pp. 343–385.

Valley, J.W., Bindeman, I.N., Peck, W.H., 2003. Empirical calibration of oxygen isotope fractionation in zircon. Geochim. Cosmochim. Acta 67, 3257–3266, doi: 10.1016/S0016-7037(03)00090-5.

Wohlers, A., Manning, C.E., Thompson, A.B., 2011. Experimental investigation of the solubility of albite and jadeite in H_2O, with paragonite + quartz at 500 and 600 °C, and 1–2.25 GPa. Geochim. Cosmochim. Acta 75, 2924–2939, doi: 10.1016/j.gca.2011.02.028.

Yui, T.-F., Fukuyama, M., 2015. A revisit to the Yorii jadeite–quartz rock, the Kanto Mountains, central Japan: Implications for petrogenesis. J. Asian Earth Sci. 108, 58–67, doi: 0.1016/j.jseaes.2015.04.022.

Yui, T.-F., Maki, K., Usuki, T., Lan, C.-Y., Martens, U.C., Wu, C.-M., Wu, T.-W., Liou, J.G., 2010. Genesis of Guatemala jadeitite and related fluid characteristics: Insight from zircon. Chem. Geol. 270, 45–55, doi: 10.1016/j.chemgeo.2009.11.004.

Yui, T.-F., Kenshi, M., Wang, K., Lan, C.-Y., Usuki, T., Iizuka, Y., Wu, C.-M., Wu, T.-W., Nishiyama, T., Martens, U.C., Liou, J.G., Grove, M., 2012. Hf isotope and REE compositions of zircon from jadeitite (Tone, Japan and north of the Motagua fault, Guatemala): Implications on jadeitite genesis and possible protoliths. Eur. J. Mineral. 24, 263–275, doi: 10.1127/0935-1221/2011/0023-2127.

Yui, T.-F., Fukoyama, M., Iizuka, Y., Wu, C.-M., Wu, T.-W., Liou, J.G., Grove, M., 2013. Is Myanmar jadeitite of Jurassic age? A result from incompletely recrystallized inherited zircon. Lithos 160–161, 268–282, doi: 10.1016/j.lithos.2012.12.011.

Zhang, Y., Wu, Y., Wang, C., Jin, Z., Schertl, H.-P., 2014. Experimental constraints on the genesis of Jadeite quartzite from Shuanghe, Dabie Mountain ultra-high pressure metamorphic terrane. Sci. China, Ser. D Earth Sci. 57 (1), 104–116, doi: 10.1007/s11430-013-4763-6.

Рекомендована
В.С. Шацким

Поступила в редакцию 5 августа 2020 г.,
принята в печать 29 января 2021 г.